

Mechanism of Asymmetric Hydrogenation of β -Dehydroamino Acids Catalyzed by Rhodium Complexes: Large-Scale Experimental and Computational Study

Ilya D. Gridnev,^{*,†,‡} Yuanyuan Liu,[‡] and Tsuneo Imamoto^{*,§}

[†]Graduate School of Science and Engineering, Tokyo Institute of Technology, 2-12-1 Ookayama, Meguro-ku, Tokyo 152-8552, Japan

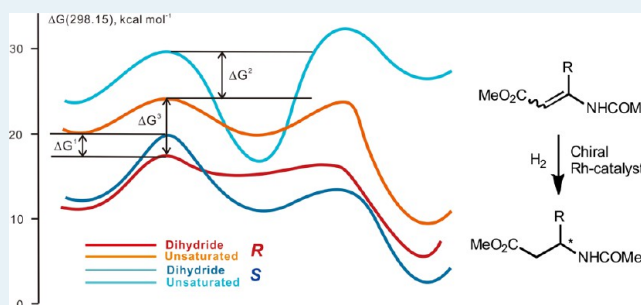
[‡]Department of Chemistry, Graduate School of Science, Tohoku University, 6-3 Aramaki, Aoba-ku, Sendai, 980-8578, Japan

[§]Department of Chemistry, Graduate School of Science, Chiba University, Yayoi-cho, Inage-ku, Chiba 263-8522, Japan

Supporting Information

ABSTRACT: The mechanism of asymmetric hydrogenation of five representative β -dehydroamino acids catalyzed by rhodium complexes of (*R*)-(tert-butylmethylphosphino)(di-tert-butylphosphino)methane (trichickenfootphos, TCFP) and (*R,R*)-1,2-bis(tert-butylmethylphosphino)benzene (BenzP*) was studied through a combination of extensive NMR experiments and state-of-the-art DFT computations in order to reveal the crucial factors governing the sense and order of enantioselectivity in this industrially important reaction. The binding mode of the substrate with a Rh(I) catalyst was found to be highly dependent on the nature of the rhodium complex and the substrate. Thus, no substrate binding was detected for $[\text{Rh}((R,R)\text{-BenzP}^*)\text{S}_2]^+\text{SbF}_6^-$ (**5**) and (*E*)-3-acetylamino-2-butenate (**2a**) even at 173 K. $[\text{Rh}((R)\text{-TCFP})\text{S}_2]^+\text{BF}_4^-$ (**3**) exhibited weak reversible binding with **2a** in the temperature interval 173–253 K with the formation of complex **4a**, whereas at ambient temperature, slow isomerization of **2a** to (*Z*)-3-acetylamino-2-butenate (**2b**) took place. The investigations with a total of 10 combinations of the catalysts and substrates demonstrated various binding modes that did not affect significantly the enantioselectivities observed in corresponding catalytic reactions and in low temperature hydrogenations of the catalyst–substrate complexes. The monohydride intermediate **10** formed quantitatively when the equilibrium mixture of **2a**, **3**, and **4a** was hydrogenated at 173 K. Its molecular structure including relative stereochemistry was determined by NMR experiments. These results together with the stereochemical outcome of the low-temperature hydrogenation (99.2% ee, *R*) and DFT calculations led to the reasonable reaction pathway of the asymmetric hydrogenation of **2a** catalyzed by **3**. The conceivable catalytic pathways were computed for five combinations of the BenzP*–Rh catalyst and prochiral β -dehydroamino acids **2a,b** and **21–23**. In most cases, it was found that the pathways involving the hydrogenation of Rh(I) square planar chelate complexes are usually higher in free energy than the pathways with the hydrogen activation prior to the chelate formation. Computed differences in the free energies of the transition states for the double bond coordination stage of the *R* and *S* pathways reasonably well reproduce the optical yields observed experimentally in the corresponding catalytic reactions and in the low temperature hydrogenation experiments. To explain extremely high ee's (>99% ee) in some of the hydrogenations, it is necessary to analyze in more detail the participation of the solvent in the enantiodetermining step.

KEYWORDS: asymmetric hydrogenation, Rh complexes, NMR spectroscopy, DFT computations, stereoselectivity, β -amino acids



INTRODUCTION

Although chiral β -amino acids are present in many natural products, they are much less common than α -amino acids. However, the synthesis of enantiopure β -amino acids is an important goal that received much attention recently since they are the building blocks for pharmaceutically important compounds, such as β -peptides or β -lactam antibiotics.¹

Catalytic asymmetric hydrogenation of prochiral β -dehydroamino acids is the most straightforward and one of the most convenient synthetic methods to provide chiral β -amino acids, and hence it has been extensively studied.² Although high selectivities can be achieved using Ru or Ir catalysts,³ the Rh-

catalyzed asymmetric hydrogenation of β -dehydroamino acids is known to operate with higher *S/C* ratios and was studied for a wider range of substrates.⁴

A well-known synthetic limitation in the Rh-catalyzed asymmetric hydrogenation is the universally lower reaction rates and optical yields obtained in the hydrogenations of more available *Z* isomers of β -dehydroamino acids.^{4–6} Besides, if the practically indefinite increase of the *S/C* ratio is possible in the

Received: September 3, 2013

Revised: December 4, 2013

Published: December 4, 2013

case of *E* isomers, the increase of the *S/C* ratio in the case of *Z* isomers often results in a rapid decrease of the optical yield and reduced rate of the reaction. Several studies were aiming to overcome this problem by looking for more effective Rh catalysts,⁵ using other metals,⁶ or preparing previously unavailable (*E*)- β -dehydroamino acids.^{4c} However, mechanistic understanding of the reactivity difference between (*E*)- and (*Z*)- β -dehydroamino acids is lacking.

On the other hand, we have been continuously interested in the mechanism of enantioselection in the Rh-catalyzed asymmetric hydrogenation,⁷ since the high orders of selectivity that are often observed in this reaction are comparable to the effectiveness of natural enzymes, and hence there is a hope of significant breakthrough in the conscious catalyst design if the intrinsic mechanism of stereoselection would be properly understood. Recent extensive experimental and computational investigations of the mechanism of Rh-catalyzed asymmetric hydrogenation of various substrates with either di-⁸ or monophosphine⁹ Rh complexes provided sufficient evidence to believe that the stereoselection takes place in octahedral Rh(III) complexes rather than in square planar Rh(I) complexes. Thus, the enantioselection-determining step is most probably the coordination of the prochiral C–C double bond to the nonchelating Rh(III) dihydride–catalyst–substrate complex. This process must involve the displacement of the coordinated solvent molecule from the coordination sphere of a metal that is not easy to account for computationally.

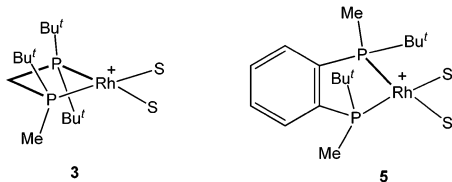
In this work, we report a large-scale experimental and computational study of the asymmetric hydrogenation of β -dehydroamino acids catalyzed by Rh complexes of (*R*)-trichickenfootphos and (*R,R*)-BenzP*. A comparative study of a wide range of high-performing reactions is beneficial for the reliable mechanistic conclusions.

RESULTS AND DISCUSSION

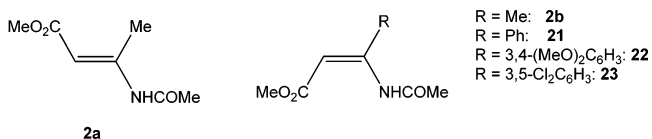
Outline of the Results and Discussion. A large amount of experimental and computational data summarized in this paper makes expedient preceding explanation of the logic of our research and the following presentation and discussion.

Experimentally, we have studied the formation of catalyst–substrate complexes between two catalysts, **3** and **5**, and five substrates, **2a**, **2b**, **21**, **22**, and **23**.

CATALYSTS



SUBSTRATES



The catalysts were chosen on the basis of their extremely high activities and enantioselectivities known for the asymmetric hydrogenation of esters of β -dehydroamino acids. On the other hand, it was interesting to check how the difference in

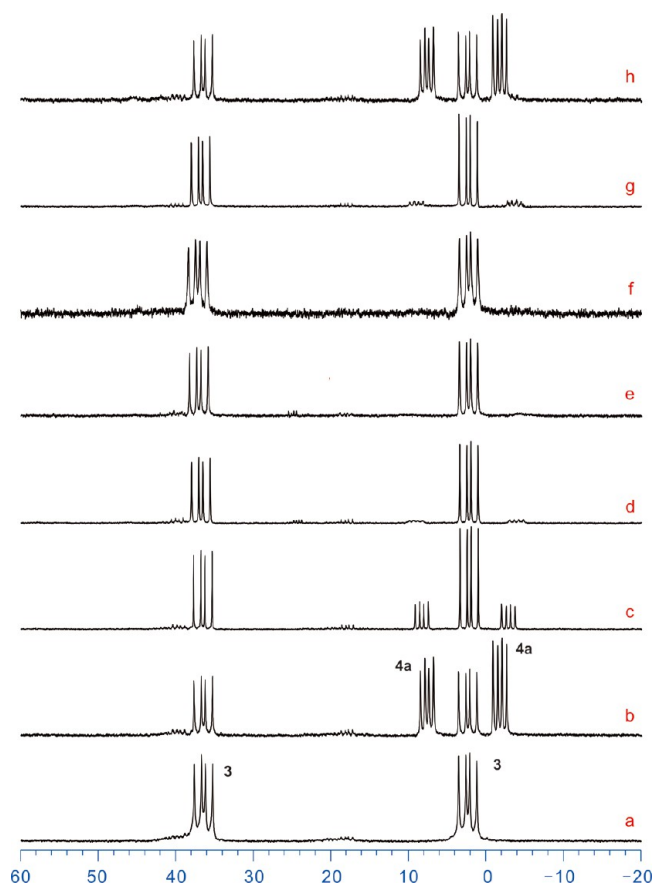
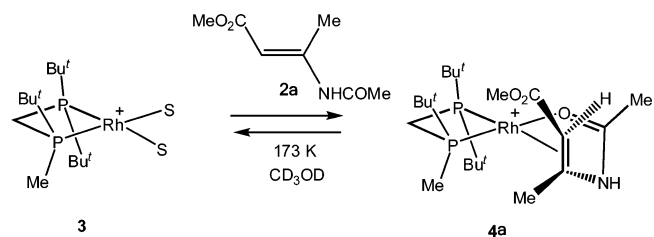
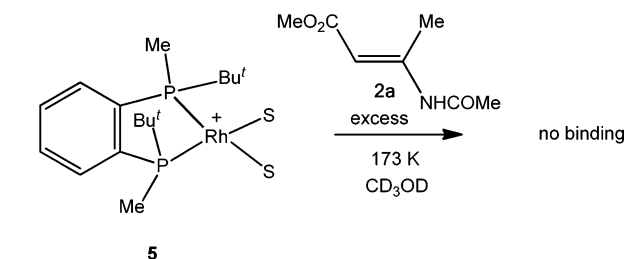


Figure 1. ³¹P NMR spectra (162 MHz, CD₃OD): (a) Of the solvate complex **3**, –100 °C; (b) after addition of 1.5 equiv of **2a**, –100 °C; (c) after raising the temperature to –70 °C; (d) after raising the temperature to –30 °C; (e) after raising the temperature to 0 °C; (f) after raising the temperature to 25 °C; (g) after recoiling to –30 °C; (h) after recoiling to –100 °C.

Scheme 1. Formation of the Catalyst–Substrate Complex 4a



Scheme 2. Lack of Binding between the Catalyst 5 and the Substrate 2a



their structure affects their binding abilities and stability of various intermediates of the catalytic cycle.

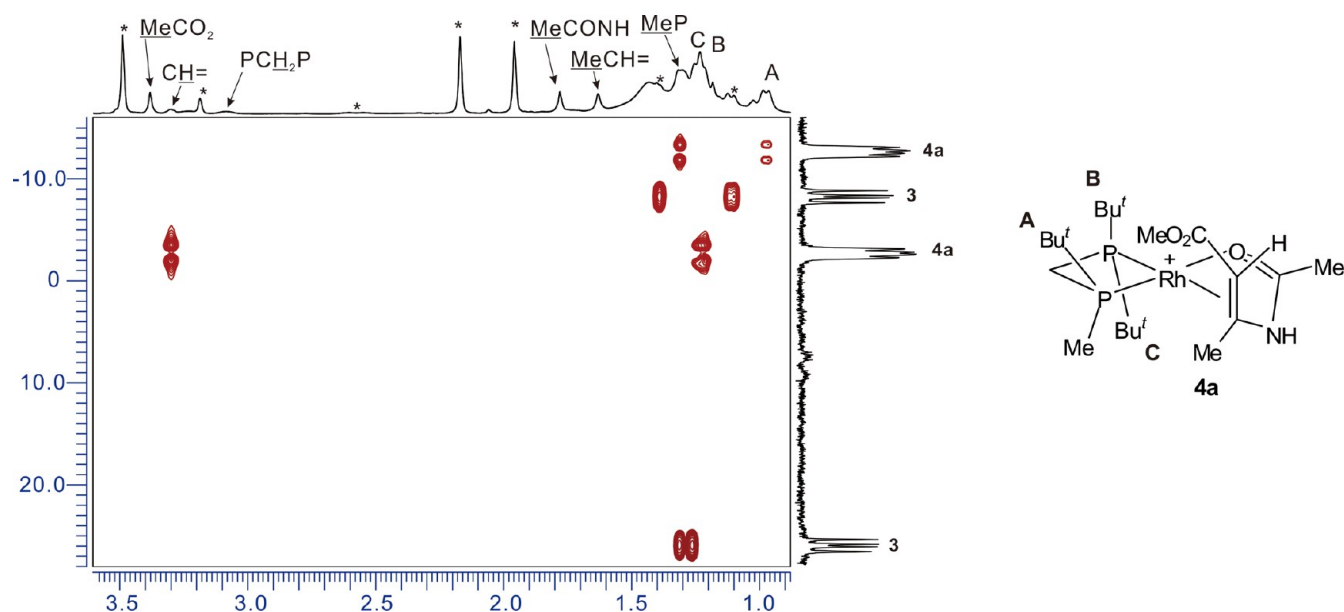


Figure 2. 2D ^1H – ^{31}P HMBC spectrum (600 MHz, CD_3OD , 178 K) of the catalyst–substrate complex **4a** in equilibrium with **3** and **2a** (signals of **3**, **2a**, and deuteriomethanol are marked with an asterisk).

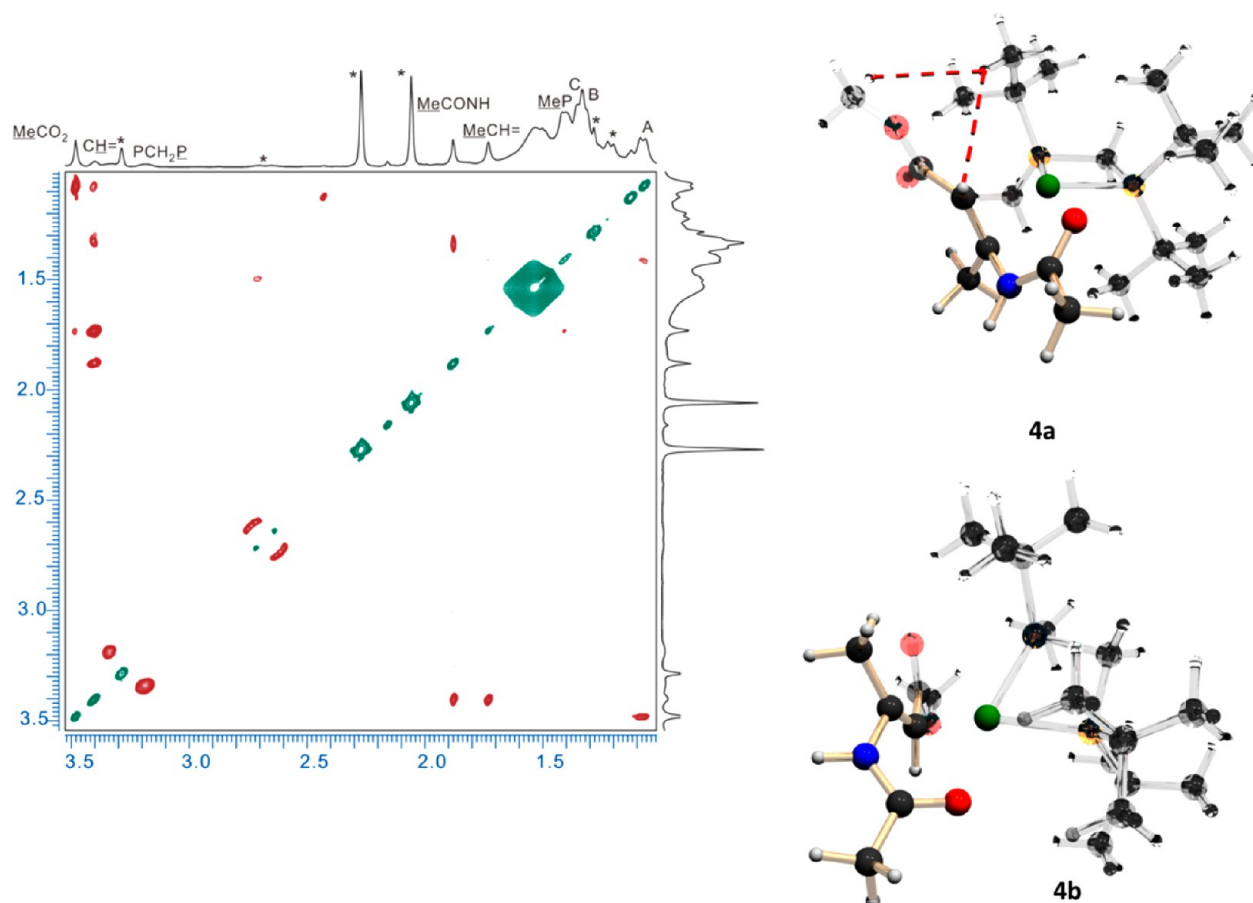
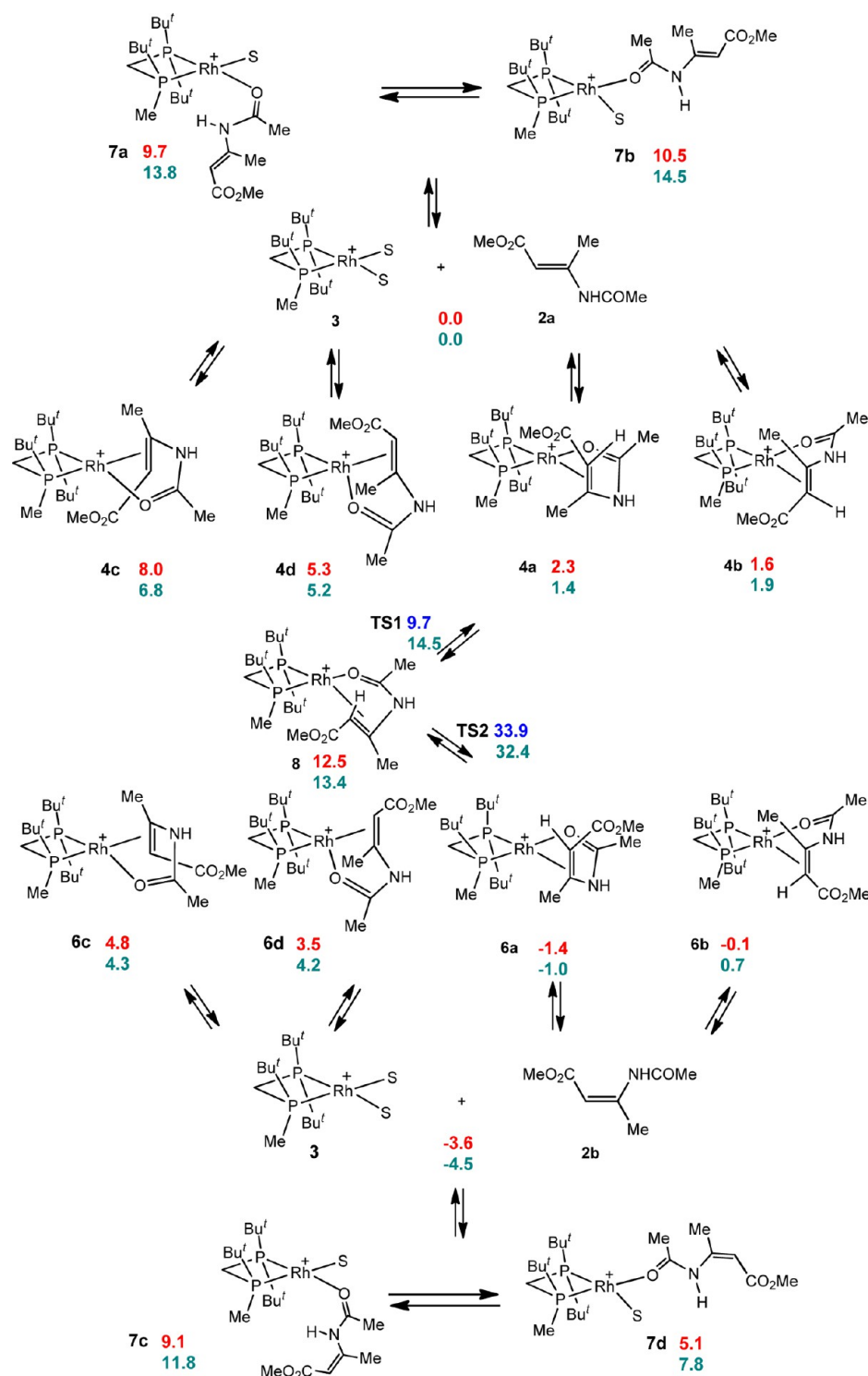


Figure 3. Phase-sensitive 2D ^1H – ^1H ROESY spectrum (600 MHz, CD_3OD , 178 K) of the catalyst–substrate complex **4a** in equilibrium with **3** and **2a** (signals of **3**, **2a**, and deuteriomethanol are marked with an asterisk). The most characteristic are ROEs of the high-field Bu^t group with $\text{CH}=\text{}$ and CH_3O groups, which are impossible in the structure **4b**. Optimized structures of **4a** and **4b** are shown for reference.

The most commonly used methyl-substituted β -dehydroamino acid esters **2a** and **2b** were complemented with three aryl-substituted β -dehydroamino acid esters **21**–**23** with different electronic properties. In particular, the substrate **23** was

interesting, because it is known to give notably lower optical yields in asymmetric hydrogenations with Rh diphosphine catalysts.

Scheme 3. Equilibria of the Square Planar Rh(I) Complexes and Computed Relative Energies of Various Species^a

^aThe numbers are relative Gibbs free energies at 298 K of intermediates (red) and transition states (blue) in kcal mol⁻¹ and relative enthalpies (green) computed at the B3LYP/SDD(Rh)/6-31G** (C, H, N, O, P)/CPCM(MeOH) level of theory.

It turned out that only **3** exhibited weak chelate binding with **2a** at decreased temperatures, whereas no binding of **5** with **2a** was detected. At ambient temperature, **3** catalyzed the isomerization of **2a** to **2b** with the formation of the corresponding chelate complexes **6a,b**. This isomerization was studied experimentally and computationally.

Since **2b** exhibited stronger binding with **3**, we hoped to detect some binding with this substrate and **5**. Indeed, the chelate complex **9** was characterized at decreased temperatures.

The combination of the catalyst **3** and substrate **2a** was found to give quantitatively upon low-temperature hydrogenation a monohydride intermediate **10** which was stable enough to be explicitly characterized at decreased temperatures. This was not

the case for any other combination catalyst–substrate; hence we used the combination 3–2a for a computational study of the possible reaction pathways leading to the experimentally observed enantiomer of the product.

These results opened the door for the computational study of the sense and order of enantioselection. However, it was more convenient to use the catalyst 5 in these computations, because unlike 3 it has C_2 symmetry that halves the number of possible isomers for any intermediate or transition state. Hence, we computed four possible pathways for each combination of 5 with five substrates and used these data for the discussion of the mechanism of enantioselection. Simultaneously, the data on the binding, catalytic hydrogenation, and low-temperature stoichiometric hydrogenation experiments were collected and summarized in Table 1.

Reaction of the Rh-Catalyst with (*E*)-3-Acetyl-amino-2-butenate. Solvate complex 3 was generated by the hydrogenation of the catalyst precursor $[\text{Rh}((R)\text{-TCFP})\text{-}(\text{cod})]^+ \text{BF}_4^-$ (1) in deuteriomethanol. The addition of 1.5 equiv of (*E*)-3-acetyl-amino-2-butenate (2a) to a precooled solution of the solvate complex 3 in deuteriomethanol resulted in a reversible formation of the catalyst–substrate complex 4a (Figure 1, Scheme 1). At 173 K, the concentrations of 3 and 4a were approximately equal (Figure 1b). Raising the temperature to 203 K dramatically decreased the equilibrium concentration of 4a (Figure 1c), and at ambient temperature 4a was not detected in the ^1H or ^{31}P NMR spectra (e.g., Figure 1f). These spectral changes were reversible: recooling of the sample brought back the spectrum shown in Figure 1a (Figure 1g,h).

The structure of the catalyst–substrate complex 4a was elucidated from the 2D correlation experiments carried out at 193 K to compromise between the concentration and adjustable resolution (Figures 2 and 3). The chemical shift of

Scheme 4. Catalytic Isomerization of 2a and 2b

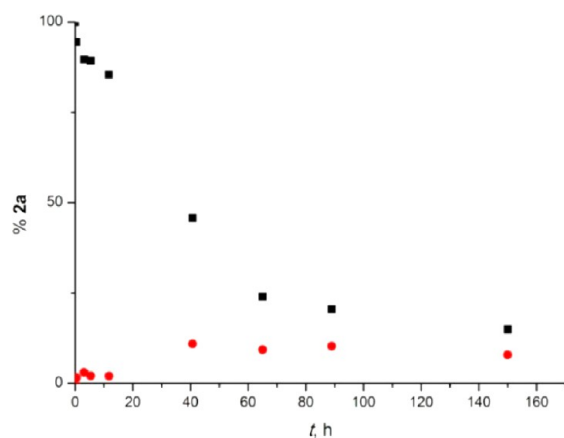
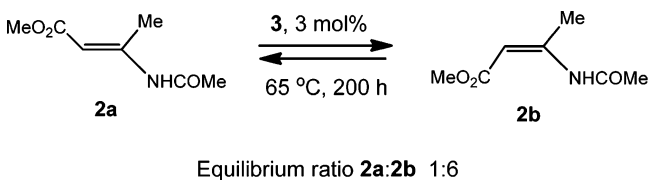


Figure 4. Kinetic curves illustrating two experiments on the catalytic isomerization starting from 2a (squares) and from 2b (dots) at 338 K (methanol- d_4 , 3 mol % of 3).

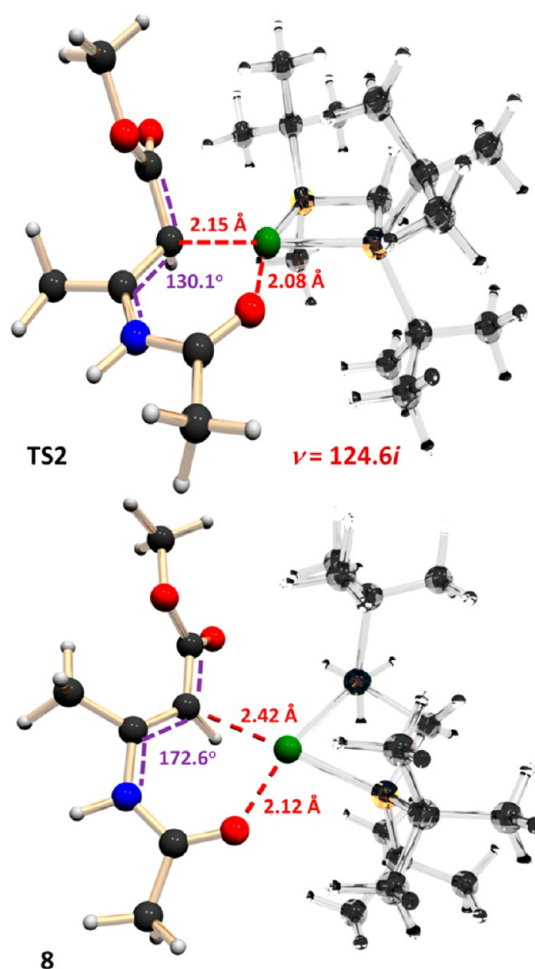


Figure 5. Optimized structures of the rate-limiting TS2 for the isomerization of 4a to 6a and of the intermediate 8. In 8, the double bond is only slightly distorted from planarity, but the mode of coordination is changed via the rotation around the MeC–NH bond. In TS2, the CH= carbon atom approaches tetrahedral configuration. The chelate binding is conserved through the reaction.

the olefinic proton in the coordinated substrate resonated at δ 3.30 that attested to the coordinated double bond. It correlated via $trans\text{-}^3J_{\text{HP}}$ with the phosphorus atom having two Bu^t groups, and hence the double bond in 4a is coordinated near the stereogenic phosphorus atom. The positions of the three nonequivalent Bu^t groups in the ^1H NMR spectrum of 4a were also found from the $^1\text{H}\text{-}^{31}\text{P}$ HMBC spectrum (Figure 2). The carbon atoms of the coordinated double bond resonated at δ 83.1 (quaternary) and 47.5 (CH=, overlapped with the signal of deuteriomethanol, located by the HMQC cross-peak). The mode of the coordination of the double bond was established from the ROESY data (Figure 3).

Thermodynamics of the binding of 2a with 3 is well reproduced by the computation data (Scheme 3). Formation of complexes 4a,b is mildly endothermic. The complex 4a is 0.5 kcal mol^{-1} more stable on the enthalpy scale, which is in accord with its selective formation at 173 K; at ambient temperature, 4b becomes slightly more stable (Scheme 3). The complexes 4c,d (with the double bond coordinated nearby the non-stereogenic phosphorus atom) are significantly less stable, similarly to the case of α -dehydroamino acids.⁷¹ These complexes were not further considered as important intermediates.

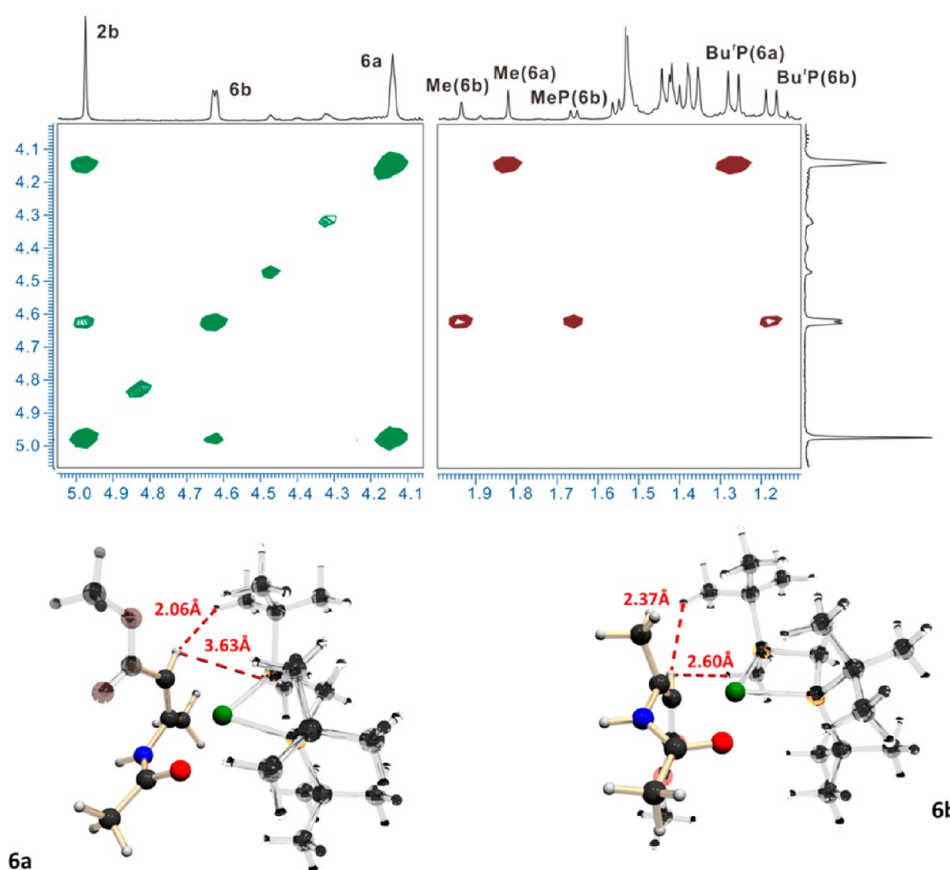


Figure 6. Section plots of phase-sensitive 2D ^1H - ^1H ROESY spectrum (600 MHz, CD_3OD , -20°C , τ_m 0.5 s) of equilibrium mixture of **3**, **2b**, **6a**, and **6b**: left, exchange cross-peaks of the $\text{CH}=\text{}$ protons; right, ROE cross-peaks of $\text{CH}=\text{}$ protons with the alkyl groups. Below: optimized structures of **6a** and **6b** (B3LYP/SDD(Rh)/6-31G(d,p)/CPCM(methanol)) and interatomic distances important for the structural assignment.

It is important to note that under the normal catalytic conditions no binding of the substrate is observed in the NMR experiments. Accordingly, the resting state of the catalytic cycle is a mixture of solvate **3** and substrate **2a**.

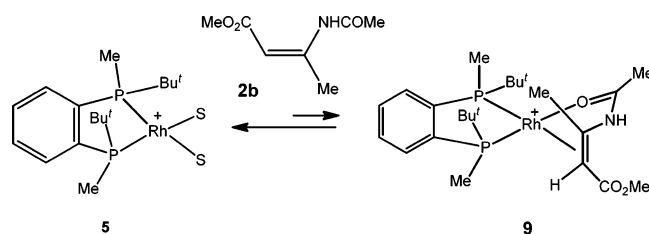
The same is valid for the catalytic system $\text{BenzP}^*\text{-Rh-2a}$. We have found that the addition of a 2-fold or 5-fold excess of **2a** to a deuteriomethanol solution of $[\text{Rh}(\text{BenzP}^*)\text{S}_2]^+$ (**5**) did not lead to the formation of any detectable complex in the temperature interval from 173 to 303 K (Scheme 2). At 173 K, the adducts were additionally sought by prolonged acquisition of a ^1H - ^{31}P HMBC spectrum, which is extremely sensitive for low concentrated species. However, no signals attributable to any analogue of **4a** were detected.

Isomerization of (E)- and (Z)-3-Acetylamino-2-butenates. Storage of the sample containing **3** and **2a** in a 1:1.5 ratio in deuteriomethanol overnight at ambient temperature resulted in the formation of two new catalyst-substrate complexes **6a,b** (Scheme 3). Besides, the signals of the (Z)-3-acetylamino-2-butenate (**2b**) were found in the ^1H and ^{13}C NMR spectra together with the signals of **2a**. (E)-3-Acetylamino-2-butenate **2a** does not bind with **3** at ambient temperature (see Figure 1 and the discussion above), hence no signals of **4a** were detected at 298 K. If the temperature of the sample was decreased to 173 K, the signals of **4a** were seen in a concentration depending on the remaining amount of **2a**. Because of the stronger binding of **2b** to **3** compared to the binding of **2a** to **3**, a sample containing only **2b**, **6a**, and **6b** could be obtained through 2 h of heating at 308 K. The

isomerization could be avoided for several days if a sample containing **3** and **2a** was kept in a freezer at 255 K.

The addition of **2b** to the solution of **3** in deuteriomethanol produced the identical complexes **6a,b**. Hence, we concluded

Scheme 5. Formation of the Catalyst-Substrate Complex **9**



that the isomerization of **2a** to **2b** took place, presumably catalyzed by **3**. Indeed, we have found that an equilibrium mixture of **2a** and **2b** is produced upon heating of either **2a** or **2b** in the presence of the catalytic amounts of **3** (Scheme 4, Figure 4).

The equilibrium ratio **2a/2b** is approximately 1:6, but the catalyst-substrate complexes **6a,b** are notably more stable than **4a,b**. No traces of **2b** were detected after 40 h of heating of a deuteriomethanol solution of **2a** at the same temperature in a blank experiment without the catalyst.

The isomerization of **2a** to **2b** did not take place when 2 equiv of **2a** was added to the solvate complex **5** and stored for 2 days at ambient temperature. However, prolonged heating at 328 K yielded the equilibrium mixture of **2a** and **2b**. Less facile

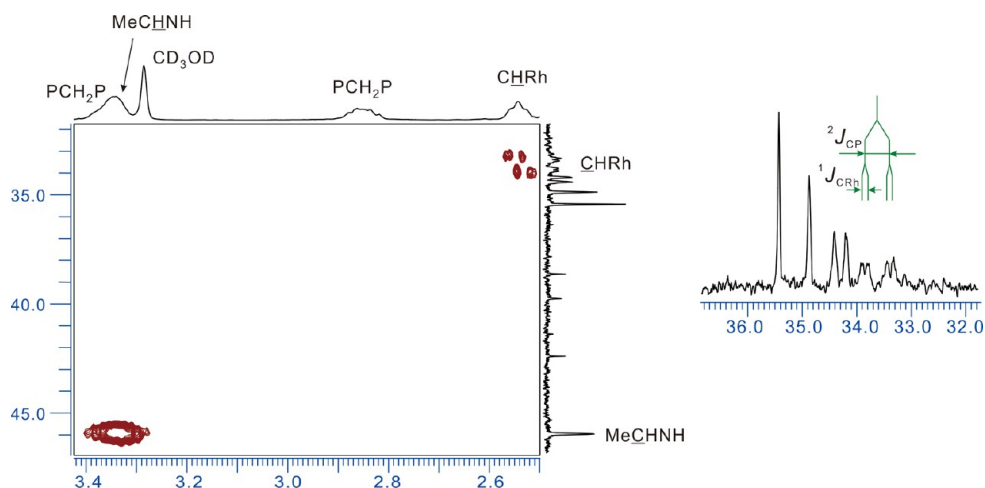


Figure 7. Section plot of 2D ^1H – ^{13}C HMQC spectrum (600 MHz, CD_3OD , 203 K) of monohydride complex **10a**. Spectrum shows cross-peaks of $\underline{\text{C}}\text{HN}$ and $\underline{\text{C}}\text{H}(\text{CO}_2\text{Me})$ carbons.

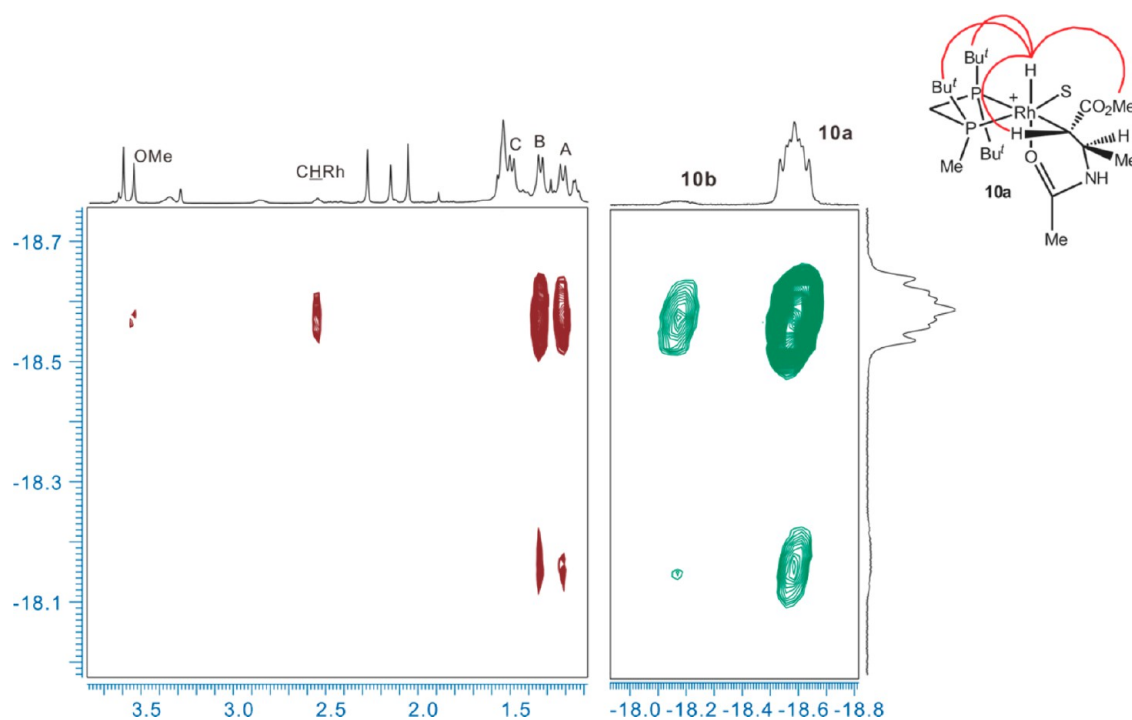


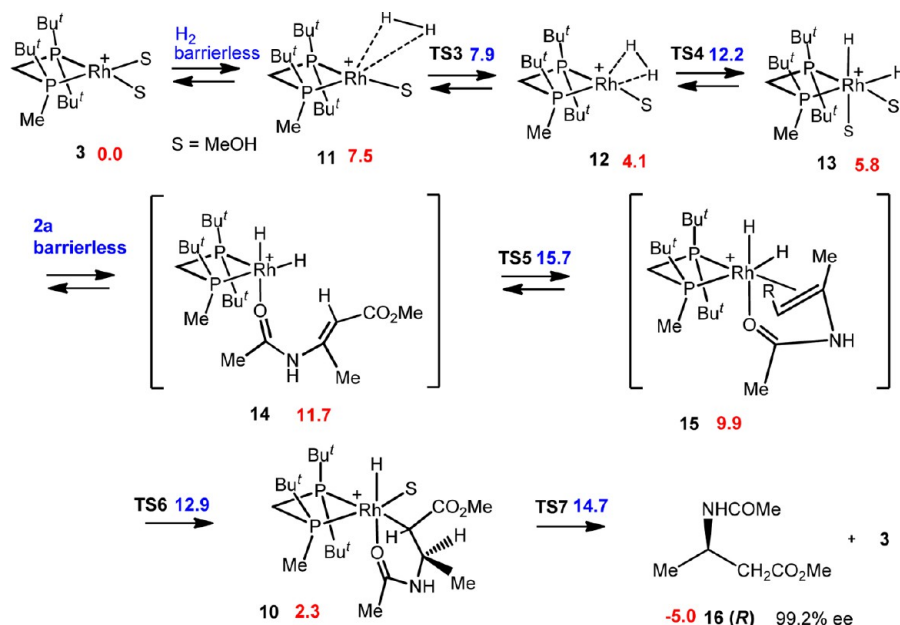
Figure 8. Section plots of phase sensitive 2D ^1H – ^1H ROESY spectrum (600 MHz, CD_3OD , 203 K) of monohydride complexes **10a,b**. The nonevident NOEs defining the structure are shown with arches. Chemical exchange between **10a** and **10b** manifests itself through green colored negative cross-peaks.

isomerization in that case is in line with the importance of the substrate binding for this isomerization that is weaker in the case of **2a** and **5**.

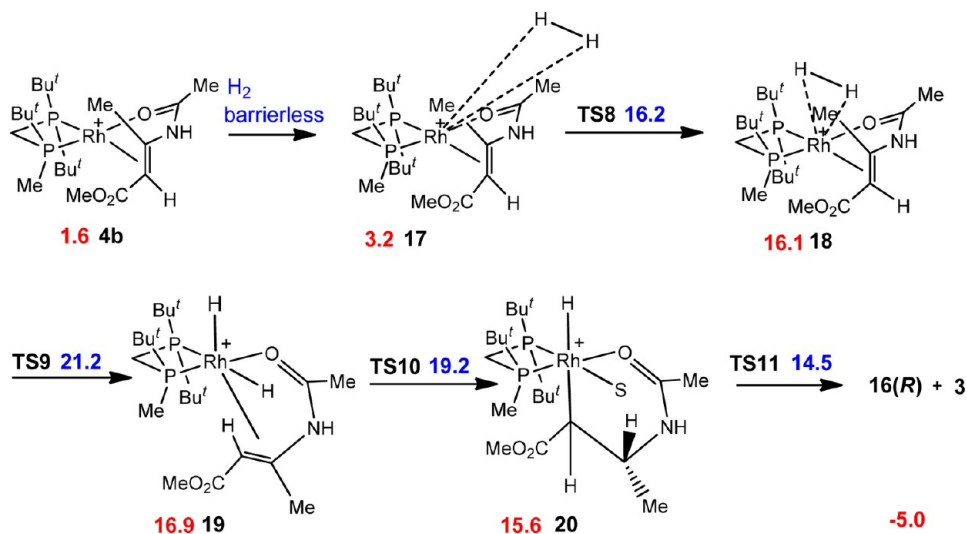
Computational analysis of the isomerization pathway afforded the transition state (Figure 5). The Intrinsic Reaction Coordinate (IRC) analysis showed that **6a** is directly connected to the rate-limiting **TS2**, however the intermediate **8** was found between **TS2** and **4a** (Scheme 3). The high activation barrier of the isomerization attests for its irrelevance to the catalytic asymmetric hydrogenation that is very fast at ambient temperature.

Structure and Interconversion of the Catalyst–Substrate Complexes 6a,b. The catalyst–substrate complexes **6a,b** exist in a solution of deuteriomethanol in a fast

equilibrium with the mixture of **3** and **2b** (Scheme 3, Figure 6). Intramolecular exchange of **6a** and **6b** does not occur, since only the exchange cross-peaks of their signals with those of **2b** in the EXSY spectrum (Figure 6) were observed at decreased temperatures. It is noteworthy that in the case of α -dehydroamino acids the intramolecular exchange of the diastereomeric catalyst–substrate complexes is usually faster than the intermolecular exchange due to the stability of the corresponding nonchelating catalyst–substrate complexes.^{7a,l} Our computations show that the corresponding nonchelate complexes **7c,d** are strongly destabilized; the same is valid for the nonchelating complexes **7a,b** in the case of the (*E*)-substrate **2a** (Scheme 3). Thus, we concluded that unlike the relatively stable nonchelating complexes in the case of α -

Scheme 6. Dihydride Reaction Pathway for the Formation of Monohydride Intermediate 10 and the Reaction Product 16(R)^a

^aThe numbers are relative free energies at 298 K of intermediates (red) and transition states (blue) in kcal mol⁻¹ computed at the B3LYP/SDD(Rh)/6-31G**(C, H, N, O, P)/CPCM(MeOH) level of theory.

Scheme 7. Unsaturated Pathway for the Formation of the Product 16(R)^a

^aThe numbers are relative free energies at 298 K of intermediates (red) and transition states (blue) in kcal mol⁻¹ computed at the B3LYP/SDD(Rh)/6-31G**(C, H, N, O, P)/CPCM(MeOH) level of theory.

dehydroamino acids, nonchelating square planar catalyst–substrate complexes are not important intermediates in the asymmetric hydrogenation of either (*E*)- or (*Z*)- β -dehydroamino acids.

The equilibrium ratio **6a**/**6b** changes from 1.5:1 at 298 K to 2.4:1 at 173 K. The double bond in the catalyst–substrate complexes **6a** and **6b** uses opposite prochiral planes for the coordination with Rh as follows from the NOE data (Figure 6).

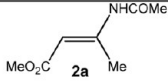
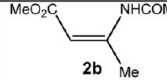
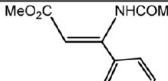
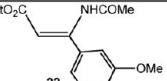
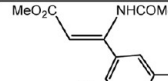
Interaction of the Solvate Complex 5 with (*Z*)-3-Acetylamino-2-butenate (2b**).** The addition of a 2-fold excess of (*Z*)-3-acetylamino-2-butenate (**2b**) to a solution of [Rh(BenzP*)S₂]⁺ SbF₆⁻ (**5**) in deuteriomethanol at -100 °C resulted in the reversible formation of a single isomer of the catalyst–substrate complex **9** (Scheme 5) that could be

observed only at decreased temperatures, whereas at the temperatures above -30 °C the equilibrium was completely shifted to the **2b** + **5** and no traces of the substrate binding could be found in the NMR spectra.

The structure of the catalyst–substrate complex **9** was elucidated from the phase-sensitive 2D ¹H–¹H ROESY experiment that attested for comparable ROE's of the CH= proton with the Me and Bu^t groups attached to the same phosphorus atom that is characteristic for the mode of coordination of the double bond similar to **2b** (see the SI for details of the ROESY experiment for **9**).

Low-Temperature Hydrogenation of the Catalyst–Substrate Complex 4a. Elucidation of the Catalytic Pathway. Hydrogenation of the equilibrium mixture of **2a**, **3**,

Table 1. Positions of Equilibria in the Samples Prepared by the Addition of 2 Equivalents of **2a** and (*Z*)- β -Dehydroamino Acids **2b**, **21–23** to Deuteriomethanol Solutions of Solvate Complexes **3** and **5**

						
3	CS complexes	4a	complexes 6a,b with opposite mode of the double bond coordination	complexes 24a,b ^a with opposite mode of the double bond coordination	complexes 26a,b with opposite mode of the double bond coordination	complexes 28a,b with opposite mode of the double bond coordination
	Position of equilibrium and isomers ratio at 298 K	No binding	Complete binding 1.5 : 1	Complete binding 1.7 : 1	Complete binding 2.5 : 1	Complete binding 1 : 1
	Optical yield cat/LT	>99%ee 99.9%ee	96%ee 79.1%ee	96.2% ee 89.8% ee	86.1% ee 88.2% ee	85% ee 85% ee
5	CS complexes	No binding	complex 9 with the mode of coordination of the double bond as in the complex 6b .	complexes 25a,b with opposite mode of the double bond coordination ^b	complexes 27a,b with opposite mode of the double bond coordination ^c	complexes 29a,b with opposite mode of the double bond coordination
	Position of equilibrium and isomers ratio at 298K	No binding	No binding	35% of 5 1 : 1.5	10% of 5 1.3 : 1	5% of 5 1 : 2.7
	Optical yield cat/LT	99.7%ee 94.7% ee	97.6%ee 71.5%ee	97.2%ee 96.3% ee	96.2% ee 96.9% ee	71% ee 90.0% ee

^aIn all cases, the mode of the coordination of the double bond for the isomers “a” and “b” was the same as in **6a** and **6b**, respectively. ^bThe isomer **25b** formed as a kinetic product when **21** was added to **5** at -100 °C; the equilibrium mixture of **25a** and **25b** formed upon raising the temperature to -30 °C. ^cBoth isomers exhibit hindered rotation of the 3,4-dimethoxyphenyl substituent at decreased temperatures.

and **4a** smoothly occurred at 173 K yielding quantitatively two monohydride intermediates **10a,b** in a ratio of 18:1. After a work-up of the sample, the hydrogenation product was of 99.2% ee (*R*).

The chemical shift of the hydride signal of **10a** ($\delta = -18.59$) and its couplings with Rh and phosphorus (14, 22, and 30 Hz) attested for the axially oriented hydride in the *trans* position to the electronegative substituent. The coupling sequence (MeO₂C)CH–CH(CH₃)–NH observed in the COSY spectrum confirmed the assignment of **10a** as β -monohydride with the Rh atom connected to the CH(CO₂Me) carbon atom. Assignment of the separate resonances for three different *t*-Bu groups in the ¹H NMR spectrum was possible from the ¹H–¹³P HMBC spectrum, and it became clear from this spectrum that the CH group bound to Rh is located *trans* to the phosphorus atom with two Bu^t substituents, since the coupling constant of this CH proton is much larger with this phosphorus atom. The carbon atom bound to Rh resonated at $\delta = 33.56$ with characteristic couplings ²J_{C–P} = 68 Hz and ¹J_{C–Rh} = 18 Hz (Figure 7). The remaining stereochemical issues were resolved by the ROEs observed in the phase sensitive 2D ¹H–¹H ROESY spectrum (Figure 8). From the section plots shown in Figure 8, it is also clear that **10b** has a structure very similar to that of **10a** and is in a rapid chemical exchange with the latter. Moreover, **10b** cannot have opposite configuration of the MeCHNH carbon atom compared to that of **10a**, since in that case the ee of the product recovered from that sample should be lower. Hence, most probably **10b** is a rotamer of **10a** with a different conformation of the carboxymethyl group in which rotation is hindered at decreased temperatures.

Quantitative formation of **10** and elucidation of its structure allowed us to follow confidently the pathway of its formation (Scheme 6). Evidently, **10** appeared after very facile (computed

$\Delta G_{298}^{\ddagger}$ 3.0 kcal mol⁻¹) migratory insertion in the dihydride intermediate **15**. The latter cannot form by a direct oxidative addition of hydrogen to a chelating catalyst–substrate complex **4b**, because the previous studies have shown that the addition of molecular hydrogen yielding a μ -H₂ complex with the appropriate configuration is precluded by high activation barriers.¹⁰ Also in our hands the only detectable pathways for oxidative addition to either **4a** or **4b** led only to the dihydride intermediates with the double bond below the chelate plane (e.g., **19**, Scheme 7). The transition state for the oxidative addition in **18** (TS9) is 5.5 kcal mol⁻¹ higher in energy than the transition state for the coordination of the double bond in **14** (TSS). Besides, when comparing the relative energies for molecular hydrides **12** and **18**, one can conclude that the concentration of the chelate species containing hydrogen in the pre-equilibrium would be negligible. In other words, in the presence of hydrogen, the equilibrium concentration of the complexes containing bound substrate decreases.

Thus, the combination of experimental and computational data allowed us to conclude reliably that the stereoselective formation of **16(R)** occurs via the dihydride pathway outlined in Scheme 6. The reaction step that determines the stereoselectivity is evidently the coordination of the double bond in **14** leading to **15**.

Although we were unable to detect any monohydride intermediate in the low-temperature NMR experiments involving hydrogenation of a 2:1 mixture of the BenzP* catalyst **5** and **2a** in deuteriomethanol at 173 K, the hydrogenation was complete within 10–15 min, and the product recovered from the sample was of 94.7% ee (*R*). Reaction pathways with relative free energies very similar to those shown in the Schemes 6 and 7 were computed for the hydrogenation of **2a** with **5** (Figure 9). On the basis of these

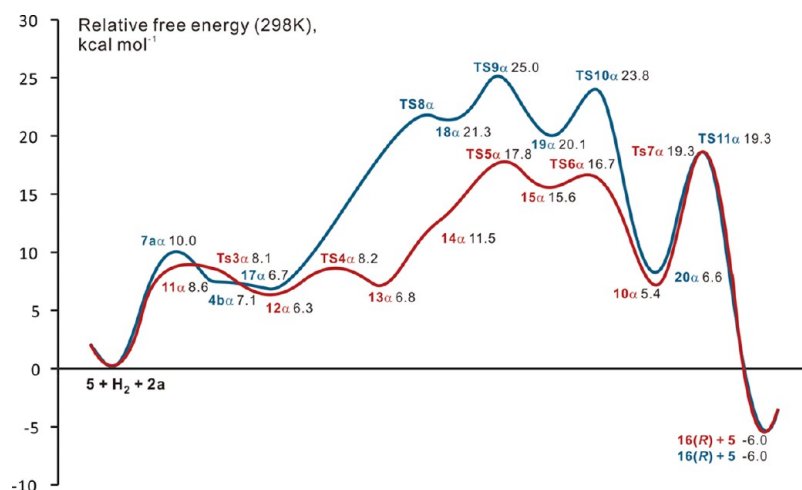
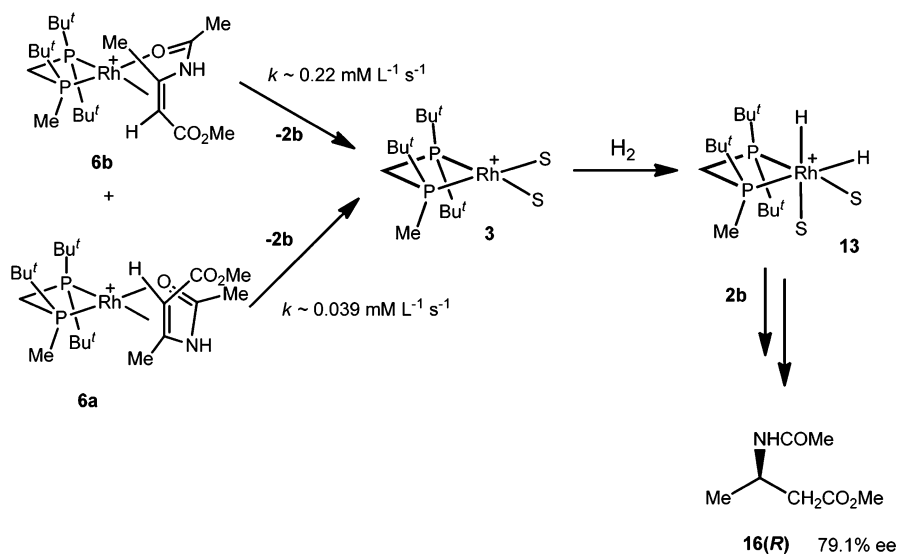


Figure 9. Potential free energy profile for two catalytic pathways leading to **16(R)** in the asymmetric hydrogenation of **2a** catalyzed with BenzP*-Rh catalyst **5** computed at the B3LYP/SDD(Rh)/6-31G***(C, H, N, O, P)/CPCM(MeOH) level of theory. The numbers of compounds and transition states correspond to those in the Schemes 6 and 7, while α denotes the system **2a**–**5**.

Scheme 8. Processes Taking Place in the Low-Temperature Hydrogenation of the Catalyst-Substrate Complexes **6a** and **6b**



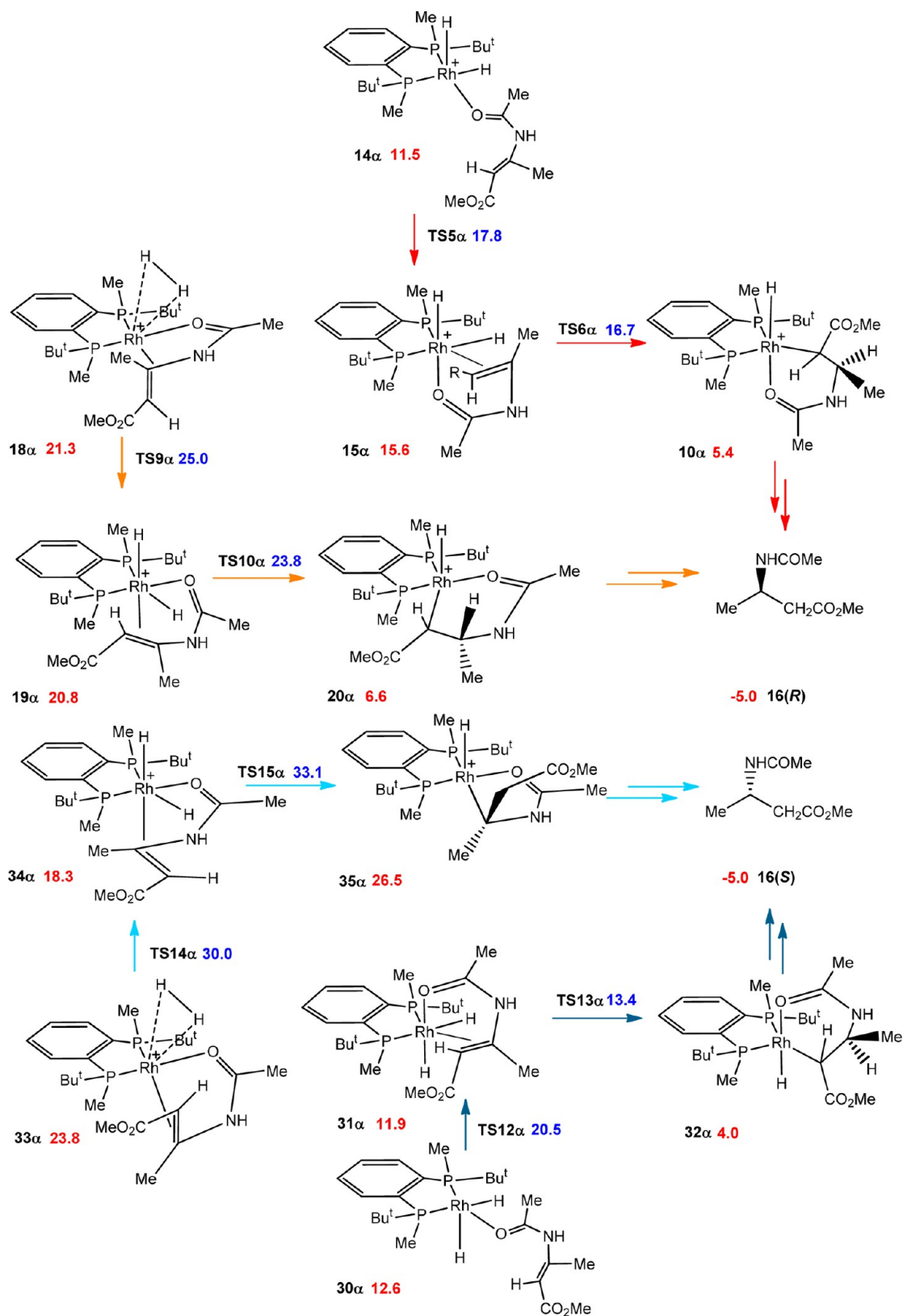
results, we have performed most of the further computations for the asymmetric hydrogenations catalyzed by **5**, since the C_1 symmetry of **3** doubles the number of conceivable intermediates that unreasonably increases the necessary computational efforts.

Low-Temperature Hydrogenation of the Catalyst-Substrate Complexes **6a,b and **9**.** The equilibrium mixture of **3**, **2b**, **6a**, and **6b** was hydrogenated at 173 K with monitoring by ^1H and ^{31}P NMR. It took 18 min to hydrogenate completely 0.1 mmol of **2b**. The ee of the product recovered from this sample was 79.1% (*R*); i.e., unlike the (*E*)-substrate **2a**, the low-temperature hydrogenation of the (*Z*)-substrate **2b** was significantly less selective than its catalytic hydrogenation. Formation of extremely unstable monohydride intermediate was detected, however it was decomposing rapidly and no concentration high enough for its characterization could be acquired. The exchange between **6a** and **6b** is slow at 173 K. Hence, the observed relative consumption rates for **6a** and **6b** do not directly correspond to the irreversible stereoselective oxidative addition, because in that case the 5-fold difference in the hydrogenation rate would result in an ee of the product of

about 60%. Rather, the different rates of the consumption of **6a** and **6b** in the low-temperature hydrogenation experiment may be explained via their different rates of dissociation to **3**, which is further hydrogenated to dihydride **13**, which in turn is rapidly consumed in the reaction with **2b** (Schemes 6 and 8); both possibilities may also interfere (vide infra).

The equilibrium mixture of **5**, **2b**, and **9** was also rapidly hydrogenated at 173 K. Only very unstable monohydride has been noticed at the early stage of hydrogenation. The ee of the hydrogenation product **16** recovered from this sample was 71.5% ee (*R*). Since direct hydrogenation of **9** would provide perfect enantioselectivity, the significant decrease of the optical yield at 173 K attests to the indirect hydrogenation via solvate dihydride.

Interaction of the Solvate Complexes **3 and **5** with (*Z*)- β -Dehydroamino Acids **21**–**23** and Low-Temperature Hydrogenation Experiments.** The results of similar experiments as described in the previous section carried out for the solvate complexes **3** and **5** and esters of (*Z*)- β -dehydroamino acids **21**–**23** are summarized in Table 1.

Scheme 9. Four Pathways for the Formation of the Products 16(R) and 16(S) in Hydrogenation of 2a Catalyzed by 5^a

^aThe numbers are relative free energies at 298 K of intermediates (red) and transition states (blue) in kcal mol⁻¹ computed at the B3LYP/SDD(Rh)/6-31G** (C, H, N, O, P)/CPCM(MeOH) level of theory.

The structures of all observable catalyst–substrate complexes were established via similar NMR experiments as it was

described above for **4a**, **6a,b**, and **9**. In the case when the aryl-substituted β -dehydroamino acids were the substrates, the

mode of coordination in a catalyst–substrate complex could be easily deduced from the significant high-field shift of the corresponding alkyl group shielded by the adjacent arene. Nevertheless, all assignments were also verified by NOESY or ROESY experiments.

From the data collected in Table 1, one can conclude that **3** exhibits stronger binding with all studied substrates than does **5**. This effect can be attributed to the fact that in the five-membered chelate cycle of **5** the bulky substituents on the phosphorus atoms hinder the space in front of the rhodium atom stronger than the same substituents of the four-membered chelate ring in **3**. The same hindrance probably retards the rotation of the 3,4-dimethoxyphenyl substituent in **27a,b**, whereas it is absent in **26a,b**.

Low-temperature hydrogenation experiments were carried out for all other combinations catalyst-substrate studied in this work. Unstable monohydride intermediates were observed in some cases, but unfortunately no quantitative formation like in the case of **10** could be confirmed in other cases. The optical yields of the reaction products obtained in these experiments compared to the ee's of the corresponding catalytic reactions are shown in Table 1. Interestingly, the significant decrease of the optical yield in the low-temperature hydrogenation experiments was observed in the case of **2b** with both catalysts, whereas for the hydrogenation of **23** catalyzed by **5** a notable increase of the optical yield was observed in the low-temperature hydrogenation. For all other substrate–catalyst combinations, very similar ee's were obtained in catalytic hydrogenations and at decreased temperatures (Table 1).

Computations of the Enantioselective Stage for Different Catalyst–Substrate Combinations. We have computed four competing pathways for each combination of the catalyst **5** with the substrates **2a**, **2b**, and **21–23**. Two of them correspond to the dihydride and unsaturated pathways described above in Schemes 6 and 7 and Figure 9. The other two pathways provide the opposite (*S*)-enantiomers via the same mechanisms (e.g., Scheme 9, Figure 10). From Figure 10, one can see that there are three characteristic values that

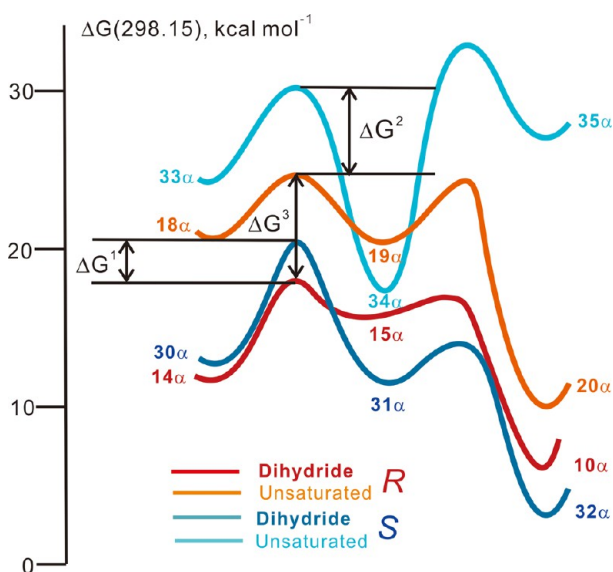


Figure 10. Sections of profiles of free energy for the enantioselective stages of the four different catalytic pathways in hydrogenation of **2a** catalyzed by **5**.

determine the enantioselectivity of the catalytic reaction: ΔG^1 , the difference in the stabilities of the transition states for the double bond recoordination (**TSS α** and **TS12 α** in the case of the hydrogenation of **2a** catalyzed by **5**); ΔG^2 , the difference in the stabilities of the transition states for the oxidative addition of H_2 to the catalyst–substrate complexes **4a** and **4b** or **6a** and **6b**; and ΔG^3 , the difference in the stabilities of the stereodetermining transition states for dihydride and unsaturated mechanisms.

The computed values of ΔG^1 , ΔG^2 , and ΔG^3 for the hydrogenation of five different substrates catalyzed by **5** are collected in Table 2 together with expected values ΔG^{exp} derived from the optical yields obtained experimentally in catalytic hydrogenation at ambient temperature and in low-temperature hydrogenations (Table 2). Thus, in the case of the hydrogenation of **2a**, the transition state for the oxidative addition of H_2 in the unsaturated pathway was computed to be $7.2 \text{ kcal mol}^{-1}$ less stable than the transition state of the double bond recoordination. This value only slightly decreases at 173 K, hence the unsaturated pathway is not interfering with the dihydride route in this case at any temperature. Hence, the optical yield of the catalytic hydrogenation of **2a** catalyzed by **5** is determined solely by the value of ΔG^1 , which was computed to be virtually the same at 298 K and at 173 K. Although the ΔG^{exp} in this case is notably higher than the computed ΔG^1 , the computations reliably reproduce the *R*-enantioselective reaction with an optical yield of about 96% ee, which is not affected by the temperature changes.

On the other hand, the computed ΔG^3 , free energy gap between dihydride and unsaturated mechanisms, is notably smaller for the hydrogenation of **2b** (Table 2). At 173 K, it is less than 3 kcal mol^{-1} , and the interference of the non-stereoselective unsaturated pathway cannot be neglected. Since, the unsaturated pathway is slightly *S*-stereoselective in this case, these computational results may explain the dramatic decrease of the ee observed in the low-temperature hydrogenation of **2b** compared to the catalytic reaction at ambient temperature.

Furthermore, these results can also explain the uniformly lower optical yields and *S/C* ratios obtained for the hydrogenation of **2b** with various catalysts when compared with the results of hydrogenation of **2a** with the same catalysts. At ambient temperature, **2b** exhibits a strong chelate binding with **3** yielding the catalyst–substrate complexes **6a,b**. Nevertheless, the free catalyst **3** is kinetically available via direct dissociation of **6a,b**, and the dihydride mechanism persists as the main catalytic pathway because the transition state for the double bond coordination within this mechanism is more stable than the transition state for the oxidative addition within unsaturated mechanism. However, the concentration of **3** can be dramatically reduced by shifting the equilibrium toward **6a,b** either by decreasing the temperature or by increasing the concentration of **2b**. In the former case, the effect of the temperature on the equilibrium is enhanced by the smaller free energy gap ΔG^3 , and the significant decrease of the optical yield is observed in the low-temperature hydrogenations. On the other hand, under the catalytic conditions the substrate **2b** is at least 100 times more concentrated than catalyst **3**, which can significantly affect the equilibrium and the order of selectivity.¹¹ A further increase of the *S/C* ratio promotes the relative importance of the *S*-stereoselective unsaturated pathway. Moreover, the rate of the reaction decreases since the more facile dihydride pathway cannot operate effectively due to the low concentration of the free

Table 2. Computed Values of the Free Energy Differences between Corresponding Transition States in the Catalytic Pathways of Hydrogenation of Various Substrates Catalyzed by BenzP*-Rh Complex **5** and Expected Values Derived from the Experimental ee Values (See Text for Details)

substrate	temperature, K	ΔG^1 , kcal mol ⁻¹	ΔG^2 , kcal mol ⁻¹	ΔG^3 , kcal mol ⁻¹	ΔG^{exp} , kcal mol ⁻¹
2a	298.15	2.7	5.0	7.2	3.8
	173.15	2.6	4.8	5.6	3.8
2b	298.15	1.9	-0.6	3.7	2.6
	173.15	2.2	-0.6	2.9	1.1
21	298.15	2.8	0.9	4.9	2.5
	173.15	2.5	0.8	3.9	2.3
22	298.15	1.5	-1.6	6.5	2.3
	173.15	1.8	-1.6	5.4	2.5
23	298.15	1.5	0.7	4.0	1.1
	173.15	1.9	0.3	3.1	1.7

catalyst. In the case of the (*E*)-substrate **2a**, the binding of the catalyst is negligible at ambient temperature, which makes it possible to increase the S/C ratio almost indefinitely without a decrease of the optical yield.

It is also worth mentioning that, evidently enough, the relative concentration of the complexes with opposite mode of the coordination of the double bond does not play any significant role in these effects. Thus, in the case of catalyst **3**, both catalyst–substrate complexes with **2b** are present in comparable concentrations, whereas only complex **9** which would provide the *R*-enantiomer upon direct oxidative addition was detected in equilibrium with **2b** and **5** at decreased temperatures. Nevertheless, both catalytic systems exhibit a very similar drop of ee in the low-temperature hydrogenation, which is even more pronounced in the latter case (Table 2).

Similar analysis of the other data collected in Table 2 shows that the experimental data are nicely reproduced computationally for the substrate **21**. Although the unsaturated mechanism in this case is just moderately *R*-stereoselective, it probably only marginally interferes with the dihydride mechanism either at 298 or 173 K and the order of enantioselection is mostly determined by the ΔG^1 values, which are quite close to the corresponding ΔG^{exp} .

The structures of the rate- and stereodetermining transition states **TS5 γ** and **TS12 γ** are compared in Figure 11 (γ denotes the system **21–5**). Both transition states are characterized by relatively low absolute values of the imaginary frequencies normal for the intramolecular movement. In both cases, the largest displacement vectors correspond to the approach of the CH=C unit to the H–Rh–H plane. In the case of **TS5 γ** , the formation of the chelate cycle occurs in the nonhindered quadrant. In the case of **TS12 γ** the Bu^t substituent hinders the formation of the chelate cycle that results in a transition state destabilized for 2.8 kcal mol⁻¹.

The computed values of ΔG^1 for the hydrogenation of **22** (1.5 and 1.8 kcal mol⁻¹ at 298 and 173 K, respectively) are somewhat lower than the corresponding ΔG^{exp} , which are 2.3 and 2.5 kcal mol⁻¹. Nevertheless, the enantioselectivity is correctly predicted. The unsaturated pathway is notably *S*-stereoselective in this case but is not competing with the dihydride pathway, since ΔG^3 values are quite high (6.5 kcal mol⁻¹ at 298 K and 5.4 kcal mol⁻¹ at 173 K).

A notably lower optical yield was observed in the catalytic hydrogenation of **23** with BenzP*-Rh catalyst **5** compared to other substrates.⁷ⁿ The ΔG^{exp} at 298 K is only 1.1 kcal mol⁻¹ in reasonable agreement with the computed value of ΔG^1 , 1.5 kcal mol⁻¹. The unsaturated pathway was computed to be still less

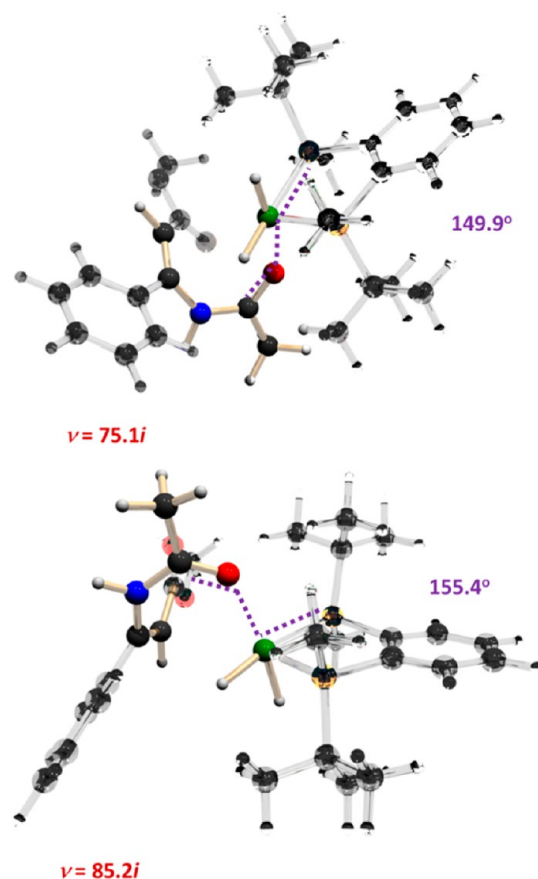
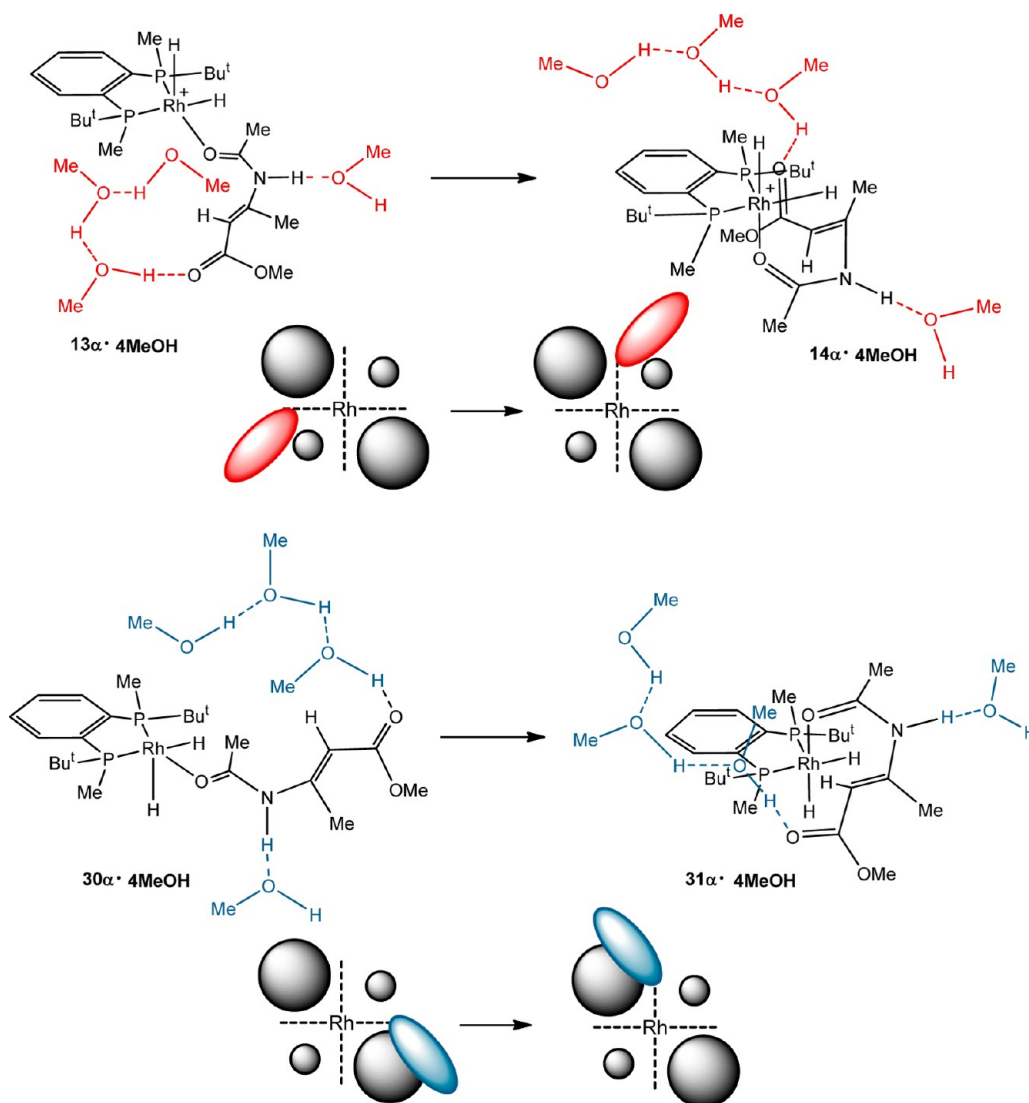


Figure 11. Optimized structures of **TS5 γ** (top) and **TS12 γ** (bottom). The larger dihedral angle is observed in **TS12 γ** , because the forming chelating cycle avoids close approach to the Bu^t group.

enantioselective (ΔG^2 , 0.7 kcal mol⁻¹), but it is unlikely to interfere in view of the reasonably high value of ΔG^3 (4.0 kcal mol⁻¹ at 298 K). Moreover, the experimentally observed increase of the ee in the low temperature hydrogenation is in agreement with the computed values of ΔG^1 at two different temperatures (Table 2).

In total, we can conclude that the delicate process of enantioselection in the asymmetric hydrogenation of β -dehydroamino acids can be roughly described as being determined by the mode of coordination of the double bond of the substrate in octahedral Rh(III) intermediates. The enantioselectivity could be correctly predicted for all studied cases if only the dihydride pathway is considered. The order of

Scheme 10. Modeling the Re-Coordination of the Double Bond with Four Methanol Molecules



enantioselection in each particular case can be affected either by the entropic effect on the activation barrier for the double bond recoordination specific for each substrate or by the interference of other catalytic pathways, e.g., the unsaturated route, which has been computed to be more energetically demanding and significantly less stereoselective in the case of (*Z*)- β -dehydroamino acids. Evidently, the interplay of different pathways must be taken into account also when rationalizing the pressure effects on the ee.¹²

Role of the Solvent in the Mechanism of Stereo-selection. In the computations summarized in the previous section, the role of solvent was accounted for by carrying out optimizations by placing the solute in a cavity within the solvent reaction field as it is implied in the CPCM model. However, it is evident that the solvent must play a more important role in the stereodetermining step, since the recoordination of the double bond implies the replacement of the solvent molecule(s) coordinated at the vacant sites of rhodium.

Recently, we have shown that introducing a molecule of methanol into the molecule of a nonchelating Rh diphosphine complex of an α -dehydroamino acid leads to very clear discrimination between *R*- and *S*-enantioselective pathways

during double bond coordination.⁷⁰ Initially, the methanol molecule was considered to occupy the vacant coordination site on the Rh atom and to be hydrogen bonded to the methoxycarbonyl group of the substrate.⁷⁰ In the case of β -dehydroamino acids, the position of the methoxycarbonyl group of the substrate is substantially different, and one methanol molecule is not enough to link it with the Rh. Hence, we have attempted to model this process by including methanol clusters in the computations (Scheme 10, Figure 11). The linear cluster containing three methanol molecules linked the methoxycarbonyl group and Rh atom. An additional methanol molecule was connected by a hydrogen bond to the NH group to prevent its eventual binding of a methanol molecule from the cluster (Scheme 10).

By scanning the relative energies on the pathways approaching the double bond to the Rh atom we have discovered that the movement of the methanol cluster occurs from the lower left nonhindered quadrant to the upper right nonhindered quadrant in the transformation of **13 α ·4MeOH** to **14 α ·4MeOH**. On the contrary, the conversion of **30 α ·4MeOH** to **31 α ·4MeOH** requires continuous movement of the methanol cluster within the hindered quadrants. Accordingly, the energy scans look out quite differently (Figure 12). The

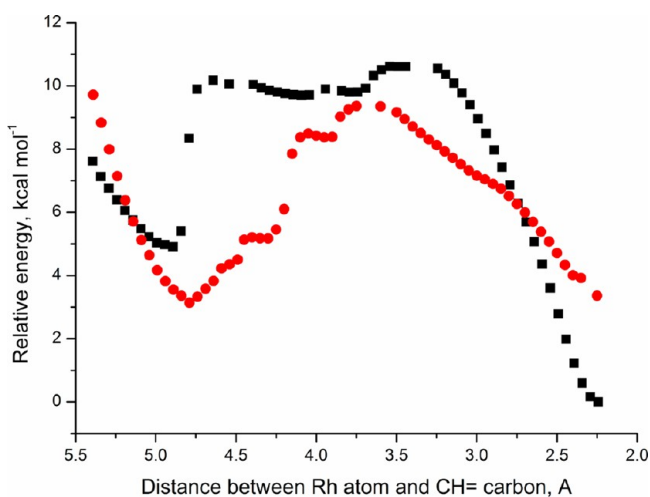


Figure 12. Scans of the relative energy changes during the approach of the CH= carbon atom to Rh. Red: from $13\alpha\cdot 4\text{MeOH}$ to $14\alpha\cdot 4\text{MeOH}$. Black: from $30\alpha\cdot 4\text{MeOH}$ to $31\alpha\cdot 4\text{MeOH}$.

scan of the former conversion can be roughly described as a potential energy profile of a single elementary step, whereas in the latter case the energy rises sharply when the C–Rh distance reaches about 5 Å and remains constantly high until 3 Å.

As a result, taking into account that all previous steps are reversible, most of the molecules with the CH= atom being 4.5 Å far away from Rh or closer will have conformation ultimately leading to $14\alpha\cdot 4\text{MeOH}$. More precisely, the relative concentrations of such molecules preceding $14\alpha\cdot 4\text{MeOH}$ and preceding $31\alpha\cdot 4\text{MeOH}$ will be determined by Boltzmann distribution for the energy difference of approximately 5 kcal mol⁻¹ (Figure 11). And this value will specify the predicted order of enantioselectivity for the dihydride pathway, rather than ~2 kcal mol⁻¹, which would be derived by optimizing the transition states from the highest points of the corresponding scans.

Unfortunately, such an approach can be hardly expected to be accurately quantified, but it demonstrates the effectiveness of this mechanism of stereoselection. In other words, the extremely high ee's that can be achieved in the hydrogenation of **2a** are not the result of a "fair competition" between the rates of similar elementary stages but the result of the effectively blocked approach to this elementary stage leading to one of the enantiomers. Remarkably, the effectiveness of this approach is not expected to depend significantly on the temperature. Hence, the uniformly high ee's in catalytic hydrogenations and low temperature experiments (as in the case of **2a** hydrogenated with **3** or **5**) can be considered as evidence of a purely dihydride mechanism. Significant changes of the optical yields with the temperature (in any direction) are explained by the admixture of competing mechanisms through natural temper-

ature variation of the rate constants in R- and S-enantioselective pathways.

CONCLUSIONS

The combined experimental and computational study of the Rh-catalyzed asymmetric hydrogenation of a representative series of (*E*)- and (*Z*)- β -dehydroamino acids revealed the sophisticated mechanism of enantioselection in this industrially important catalytic reaction. In the case of the (*E*)- β -dehydroamino acid **2a**, the single catalytic pathway is viable in the wide temperature range. This pathway does not involve the chelate substrate binding until the very late irreversible migratory insertion step that fixes the results of the enantioselective double bond coordination in the octahedral Rh(III) dihydride. Accordingly, the strong substrate binding to the catalyst is unnecessary, moreover, it can spoil the enantioselectivity by interference of another mechanism and reduce the rate of the reaction by decreasing the concentration of the free catalyst.

In the case of (*Z*)- β -dehydroamino acids, the free energy gap between two computed pathways becomes smaller, which makes possible the interference of the unsaturated mechanism, especially with increasing of the S/C ratio. Since the unsaturated mechanism was computed to be much less stereoselective, this explains the uniformly lower ee's obtained for these substrates and the difficulties in achieving their enantioselective hydrogenations with high S/C ratios.

EXPERIMENTAL SECTION

General Procedures. All reactions and manipulations were performed under a dry argon atmosphere using standard Schlenk-type techniques. NMR experiments were carried out on JEOL ESX 400, Bruker Avance 500, Jeol ESX 600, and Bruker Avance 700 spectrometers. Methanol-*d*₄ of the grade "100%" (99.6% D) packed in sealed ampules was purchased from Cambridge Isotope Laboratories, Inc. Hydrogen of 99.9999% (Tanuma Sanso) was used for the mechanistic studies.

Solvate Complex 3. A solution of catalytic precursor **1** (20–40 mg) in 0.5 mL of CD₃OD was prepared in a 5 mm NMR tube under argon. Then, the sample was degassed by three consequent cycles of freezing, pumping, and warming. The sample was cooled to –20 °C, and 2 atm of H₂ was admitted, and the temperature was raised to ambient. The sample was intensively shaken manually during the hydrogenation at ambient temperature. The progress of hydrogenation was monitored by ³¹P NMR; complete hydrogenation of the coordinated COD required 60–90 min at room temperature. After completion of the reaction, the excessive hydrogen was removed by several consequent cycles of freezing, pumping, and warming. The thus-prepared solution of solvate complex **3** in deuteriomethanol was stable at ambient temperature.

Table 3. Chemical Shifts (δ) and Coupling Constants (Hz) in the ³¹P NMR Spectra (243 MHz, CD₃OD) of the Catalyst–Substrate Complexes Made by the Catalyst **3** with Various Substrates

compound ^a	3 + 2a ^b	3 + 2b ^c		3 + 21		3 + 22		3 + 23	
		re	si	re	si	re	si	re	si
δ_{P-1} (¹ J _{RhP})	–12.77(135)	–14.64(140)	–16.33(132)	–14.90(141)	–17.44(146)	–14.61(142)	–17.40(130)	–16.34 (135)	–17.70 (125)
δ_{P-2} (¹ J _{RhP})	–2.57(138)	–2.44(138)	–2.51(141)	–2.06(148)	–1.09(147)	–2.03(142)	–1.09(140)	–2.70 (138)	–1.22 (135)
² J _{PP}	81	75	90	76	89	75	86	85	85

^aFor these complexes, re and si are indicated at the carbon atom attached to the acetylamino group. ^bAt 183 K. ^cAt 273 K.

Table 4. Chemical Shifts (δ) and Coupling Constants (Hz) in the ^{31}P NMR Spectra (243 MHz, CD_3OD) of the Catalyst–Substrate Complexes Made by the Catalyst 5 with Various Substrates

compound ^a	5 + 2b ^b	5 + 21 ^c		5 + 22 ^d		5 + 23	
		re	si	re	si ^e	re	si
$\delta_{\text{P-1}}$ ($^1J_{\text{RhP}}$)	54.62(165)	54.17(171)	61.69(167)	54.66(166)	59.93(170) 61.40(165)	54.47(162)	62.24(158)
$\delta_{\text{P-2}}$ ($^1J_{\text{RhP}}$)	66.23(159)	66.17(164)	70.09(152)	66.784(155)	69.89(152) 70.19(152)	64.01(166)	69.18(151)
$^2J_{\text{PP}}$	26	28	40	33	39, 41	31	43

^aFor these complexes, re and si are indicated at the carbon atom attached to the acetyl amino group. ^bAt 178 K. ^cAt 298 K. ^dAt 223 K. ^eTwo rotamers in a 1.4:1 ratio.

Catalyst–Substrate Complexes. Two equivalents of a prochiral substrate were added to a sample containing a solution of **3** or **5** in deuteriomethanol precooled to 173 K. Then, the sample was transferred to the probe of a NMR spectrometer precooled to 173 K. The ^{31}P NMR spectra of the catalyst–substrate complexes are listed in the Tables 3 and 4. The listings of the ^1H and ^{13}C NMR spectra can be found in the Supporting Information (Tables S1–S4).

Hydrogenation Experiments. The temperature of the cooling bath was maintained at $-100\text{ }^\circ\text{C}$ (liquid nitrogen + ether), the sample connected to the rubber balloon with dihydrogen was manually kept inside the bath throughout the whole hydrogenation process. To provide the necessary mass transfer, the sample has been intensively shaken manually.

Monohydride Intermediate 10a. ^1H NMR (600 MHz, CD_3OD , 203 K): δ -18.59 (ddd, 1H, Rh–H, $^1J_{\text{RhH}} = 11$, 21, 31 Hz), 1.15 (d, 3H, CH_3 , $^3J_{\text{HH}} = 6$ Hz), 1.21 (d, 9H, $\text{C}(\text{CH}_3)_3$, $^3J_{\text{HP}} = 16$ Hz), 1.34 (d, 9H, $\text{C}(\text{CH}_3)_3$, $^3J_{\text{HP}} = 14$ Hz), 1.49 (d, 9H, $\text{C}(\text{CH}_3)_3$, $^3J_{\text{HP}} = 14$ Hz), 1.56 (d, 3H, CH_3 , $^2J_{\text{HP}} = 8$ Hz), 2.14 (s, 3H, CH_3CONH), 2.54 (dd, 1H, CHRh, $^2J_{\text{RhH}} \approx ^3J_{\text{HH}} = 8$ Hz), 2.85 (m, 1H of PCH_2P), 3.34 (m, 1H, CHCH_3), 3.38 (m, 1H of PCH_2P), 3.54 (s, 3H, OCH_3). ^{31}P NMR (243 MHz, CD_3OD , 203 K): δ 13.07 (dd, $^1J_{\text{PRh}} = 82$ Hz, $^2J_{\text{PP}} = 46$ Hz), 28.4 (dd, $^1J_{\text{PRh}} = 130$ Hz, $^2J_{\text{PP}} = 46$ Hz). ^{13}C NMR (150 MHz, CD_3OD , 203 K): δ 6.55 (d, CH_3P , $^1J_{\text{CP}} = 22$ Hz), 18.97 (d, CH_3CH , $^4J_{\text{CP}} = 9$ Hz), 21.16 ($\underline{\text{C}}\text{H}_3\text{CONH}$), 24.73 ($\underline{\text{C}}\text{H}_3$)₃C, 28.71 ($\underline{\text{C}}\text{H}_3$)₃C, 28.93($\underline{\text{C}}\text{H}_3$)₃C, 29.19 (m, CH_2), 33.56 (dd, CRh, $^2J_{\text{CP}} = 68$ Hz, $^1J_{\text{CRh}} = 18$ Hz), 34.30 (d, CH_3)₃C, $^1J_{\text{CP}} = 34$ Hz), 34.87 ($\underline{\text{C}}\text{H}_3$)₃C, 35.46 ($\underline{\text{C}}\text{H}_3$)₃C, 45.96 ($\underline{\text{C}}\text{HNH}$), 50.07 (OCH_3), 171.55 ($\text{NH}\underline{\text{C}}\text{O}$), 181.73 ($\text{CH}_3\text{O}\underline{\text{C}}$).

Computational Details. All computations were carried out using the hybrid Becke functional (B3)¹³ for electron exchange and the correlation functional of Lee, Yang, and Parr (LYP),¹⁴ as implemented in the Gaussian 09 software package.¹⁵ For rhodium, the SDD basis set with the associated effective core potential was employed.¹⁶ All other atoms were modeled at the 6-31G(d,p) level of theory.¹⁷ The following additional diffuse function was applied for the phosphorus atom:

P 0
D 1 1.0
0.55 0.100D+01

Geometry optimizations were performed with the account of the solvent effects (CPCM, methanol) without applying any geometry constraints (C_1 symmetry).

Starting geometries for the transition state search were located either by QST2 or by QST3 procedures, or by the guess based on the structure of the previously found TS. The transition states were subsequently fully optimized as saddle

points of first order, employing the Berny algorithm. Frequency calculations were carried out to confirm the nature of the stationary points, yielding zero imaginary frequencies for all Rh complexes and one imaginary frequency for all transition states, which represented the vector for the appropriate bond formation.

■ ASSOCIATED CONTENT

📄 Supporting Information

NMR tables, NMR charts, complete reference¹⁴, and Cartesian coordinates of the optimized structures. This material is available free of charge via the Internet at <http://pubs.acs.org>.

■ AUTHOR INFORMATION

✉ Corresponding Authors

*E-mail: igradnev@m.tohoku.ac.jp.

*E-mail: imamoto@faculty.chiba-u.jp.

📌 Notes

The authors declare no competing financial interest.

■ ACKNOWLEDGMENTS

This work was financially supported by the Global COE Program of Tokyo Institute of Technology and by the Campus Asia Program of Tohoku University. Computational results in this research were obtained using supercomputing resources at the Information Synergy Center, Tokyo Institute of Technology. We thank Nippon Chemical Industrial Co., Ltd. for a generous donation of the $\text{BenzP}^*\text{-Rh}$ complex and β -dehydroamino acid esters. This paper is dedicated to Professor Teruaki Mukaiyama in celebration of the 40th anniversary of the Mukaiyama aldol reaction.

■ REFERENCES

- (1) (a) von Nussbaum, F.; Spittler, P. In *Highlights in Bioorganic Chemistry: Methods and Application*; Schmuck, C., Wennemers, H., Eds.; Wiley-VCH: Weinheim, Germany, 2004; pp 63–89. (b) *Enantioselective Synthesis of β -Amino Acids*; Juaristi, E., Soloshonok, V., Eds.; John Wiley & Sons Inc.: Hoboken, NJ, 2005.
- (2) For some recent representative reviews, see: (a) Liu, M.; Sibi, M. P. *Tetrahedron* **2002**, *58*, 7991–8035. (b) Ma, J.-A. *Angew. Chem., Int. Ed.* **2003**, *42*, 4290–4299. (c) Bruneau, C.; Renaud, J.-L.; Jerphagnon, T. *Coord. Chem. Rev.* **2008**, *252*, 532–544. (d) Weiner, B.; Szymański, W.; Janssen, D. B.; Minnaard, A. J.; Feringa, B. L. *Chem. Soc. Rev.* **2010**, *39*, 1656–1691. (e) Xie, J.-H.; Zhu, S.-F.; Zhou, Q.-L. *Chem. Rev.* **2011**, *111*, 1713–1760.
- (3) Ru examples: (a) Lubell, W. D.; Kitamura, M.; Noyori, R. *Tetrahedron: Asymmetry* **1991**, *2*, 543–554. (b) Wu, J.; Chen, X.; Guo, R.; Yeung, C.-H.; Chan, A. S. C. *J. Org. Chem.* **2003**, *68*, 2490–2493. (c) Qiu, L.; Wu, J.; Chan, S.; Au-Yeung, T. T.-L.; Ji, J.-X.; Guo, R.; Pai, C.-C.; Zhou, Z.; Li, X.; Fan, Q.-H.; Chan, A. S. C. *Proc. Natl. Acad. Sci. U. S. A.* **2004**, *101*, 5815–5820. (d) Qiu, L.; Kwong, F. Y.; Wu, J.;

Lam, W. H.; Chan, S.; Yu, W.-Y.; Li, Y.-M.; Guo, R.; Zhou, Z.; Chan, A. S. C. *J. Am. Chem. Soc.* **2006**, *128*, 5955–5965. Ir examples: (e) Enthaler, S.; Erre, G.; Junge, K.; Schröder, K.; Addis, D.; Michalik, D.; Hapke, M.; Redkin, D.; Beller, M. *Eur. J. Org. Chem.* **2008**, 3352–3362.

(4) Zhu, G.; Chen, Z.; Zhang, X. *J. Org. Chem.* **1999**, *64*, 6907–6910. (b) Yasutake, M.; Gridnev, I. D.; Higashi, N.; Imamoto, T. *Org. Lett.* **2001**, *3*, 1701–1704. (c) You, J.; Drexler, H.-J.; Zhang, S.; Fischer, C.; Heller, D. *Angew. Chem., Int. Ed.* **2003**, *42*, 913–916. (d) Tang, W.; Wang, W.; Chi, Y.; Zhang, X. *Angew. Chem., Int. Ed.* **2003**, *42*, 3509–3511. (e) Fu, Y.; Hou, G.-H.; Xie, J.-H.; Xing, L.; Wang, L.-X.; Zhou, Q.-L. *J. Org. Chem.* **2004**, *69*, 8157–8160. (f) Dubrovina, N. V.; Tararov, V. I.; Monsees, A.; Spannenberg, A.; Kostas, I. D.; Börner, A. *Tetrahedron: Asymmetry* **2005**, *16*, 3640–3649. (g) Reetz, M. T.; Li, X. *Angew. Chem., Int. Ed.* **2005**, *44*, 2959–2962. (h) Tamura, K.; Sugiya, M.; Yoshida, K.; Yanagisawa, A.; Imamoto, T. *Org. Lett.* **2010**, *12*, 4400–4403. (i) Zhang, Z.; Tamura, K.; Mayama, D.; Sugiya, M.; Imamoto, T. *J. Org. Chem.* **2012**, *77*, 4184–4188.

(5) (a) Tang, W.; Zhang, X. *Org. Lett.* **2002**, *4*, 4159. (b) Lee, S.-G.; Zhang, Y. *J. Org. Lett.* **2002**, *4*, 2429–2431. (c) Peña, D.; Minnaard, A. J.; de Vries, J. G.; Feringa, B. L. *J. Am. Chem. Soc.* **2002**, *124*, 14552–14553. (d) Tang, W.; Wang, W.; Chi, Y.; Zhang, X. *Angew. Chem., Int. Ed.* **2003**, *42*, 3509–3511. (e) Wu, H.-P.; Hoge, G. *Org. Lett.* **2004**, *6*, 3645–3647. (f) Lefort, L.; Boogers, J. A. F.; de Vries, A. H. M.; de Vries, J. G. *Org. Lett.* **2004**, *6*, 1733. (g) Hu, X.-P.; Zheng, Z. *Org. Lett.* **2005**, *7*, 419–422. (h) Tang, W.; Capacci, A. G.; White, A.; Ma, S.; Rodriguez, S.; Qu, B.; Savoie, J.; Patel, N. D.; Wei, X.; Haddad, N.; Grinberg, N.; Yee, N. K.; Krishnamurthy, D.; Senanayake, C. H. *Org. Lett.* **2010**, *12*, 1104–1107. (i) Zhang, X.; Huang, K.; Hou, G.; Cao, B.; Zhang, X. *Angew. Chem., Int. Ed.* **2010**, *49*, 6421–6424.

(6) (a) Zhou, Y.-G.; Tang, W.; Wang, W.-B.; Li, W.; Zhang, X. *J. Am. Chem. Soc.* **2002**, *124*, 4952–4953. (b) Wu, Y.; Qi, S.-B.; Wu, F.-F.; Zhang, X.-C.; Li, M.; Wu, J.; Chan, A. S. C. *Org. Lett.* **2011**, *7*, 1754–1757.

(7) (a) Gridnev, I. D.; Higashi, N.; Asakura, K.; Imamoto, T. *J. Am. Chem. Soc.* **2000**, *122*, 7183–7194. (b) Gridnev, I. D.; Higashi, N.; Imamoto, T. *J. Am. Chem. Soc.* **2000**, *122*, 10486–10487. (c) Gridnev, I. D.; Imamoto, T. *Organometallics* **2001**, *20*, 545–549. (d) Gridnev, I. D.; Yamanoi, Y.; Higashi, N.; Tsuruta, H.; Yasutake, M.; Imamoto, T. *Adv. Synth. Catal.* **2001**, *343*, 118–136. (e) Gridnev, I. D.; Higashi, N.; Imamoto, T. *Organometallics* **2001**, *20*, 4542–4553. (f) Gridnev, I. D.; Yasutake, M.; Higashi, N.; Imamoto, T. *J. Am. Chem. Soc.* **2001**, *123*, 5268–5276. (g) Gridnev, I. D.; Higashi, N.; Imamoto, T. *J. Am. Chem. Soc.* **2001**, *123*, 4631–4632. (h) Gridnev, I. D.; Yasutake, M.; Imamoto, T.; Beletskaya, I. P. *Proc. Natl. Acad. Sci. U. S. A.* **2004**, *101*, 5385–5390. (i) Wada, Y.; Imamoto, T.; Tsuruta, H.; Yamaguchi, K.; Gridnev, I. D. *Adv. Synth. Catal.* **2004**, *346*, 777–788. (j) Tsuruta, H.; Imamoto, T.; Yamaguchi, K.; Gridnev, I. D. *Tetrahedron Lett.* **2005**, *46*, 2879–2882. (k) Imamoto, T.; Yashio, K.; Crépy, K. V. L.; Katagiri, K.; Takahashi, H.; Kouchi, M.; Gridnev, I. D. *Organometallics* **2006**, *25*, 908–914. (l) Gridnev, I. D.; Imamoto, T.; Hoge, G.; Kouchi, M.; Takahashi, H. *J. Am. Chem. Soc.* **2008**, *130*, 2560–2572. (m) Imamoto, T.; Itoh, T.; Yoshida, K.; Gridnev, I. D. *Chem.—Asian J.* **2008**, *3*, 1636–1641. (n) Imamoto, T.; Tamura, K.; Zhang, Z.; Horiuchi, Y.; Sugiya, M.; Yoshida, K.; Yanagisawa, A.; Gridnev, I. D. *J. Am. Chem. Soc.* **2012**, *134*, 1754–1769. (o) Gridnev, I. D.; Kohrt, C.; Liu, Y. *Dalton Trans.* **2013**, DOI: 10.1039/C3DT52383G.

(8) Reviews: (a) Gridnev, I. D.; Imamoto, T. *Acc. Chem. Res.* **2004**, *37*, 633–644. (b) Gridnev, I. D.; Imamoto, T. *Chem. Commun.* **2009**, 7447–7464.

(9) (a) Gridnev, I. D.; Fan, C.; Pringle, P. G. *Chem. Commun.* **2007**, 1319–1321. (b) Shuklov, I. A.; Dubrovina, N. V.; Barsch, E.; Ludwig, R.; Michalik, D.; Börner, A. *Chem. Commun.* **2009**, 1535–1537. (c) Jankowski, P.; McMullin, C. L.; Gridnev, I. D.; Orpen, A. G.; Pringle, P. G. *Tetrahedron: Asymmetry* **2010**, *21*, 1206–1209. (d) Schiaffino, L.; Ercolani, G. *J. Phys. Org. Chem.* **2011**, *24*, 257–261. (e) Alberico, E.; Baumann, W.; de Vries, J. G.; Drexler, H.-J.; Gladiali, S.; Heller, D.; Henderickx, H. J. W.; Lefort, L. *Chem.—Eur. J.*

2011, *17*, 12683–12695. (f) Gridnev, I. D.; Alberico, E.; Gladiali, S. *Chem. Commun.* **2012**, 2186–2188.

(10) (a) Landis, C. R.; Hilfenhaus, P.; Feldgus, S. *J. Am. Chem. Soc.* **1999**, *121*, 8741–8754. (b) Landis, C. R.; Feldgus, S. *Angew. Chem., Int. Ed.* **2000**, *39*, 2863–2866. (c) Feldgus, S.; Landis, C. R. *J. Am. Chem. Soc.* **2000**, *122*, 12714. (d) Feldgus, S.; Landis, C. R. *Organometallics* **2001**, *20*, 2374–2386.

(11) Drexler, H.-J.; Baumann, W.; Schmidt, T.; Zhang, S.; Sun, A.; Spannenberg, A.; Fischer, C.; Buschmann, H.; Heller, D. *Angew. Chem., Int. Ed.* **2005**, *44*, 1184–1188.

(12) Aloui, A.; Delbeck, F.; Sautet, P.; De Bellefon, C. *J. Mol. Catal. A: Chem.* **2012**, 363–364, 214–222.

(13) (a) Becke, A. D. *J. Chem. Phys.* **1993**, *98*, 1372–1377. (b) Becke, A. D. *J. Chem. Phys.* **1993**, *98*, 5648–5652.

(14) Lee, C.; Yang, W.; Parr, R. G. *Phys. Rev. B* **1988**, *37*, 785–789.

(15) Frisch, M. J.; Trucks, G. W.; Schlegel, H. B.; Scuseria, G. E.; Robb, M. A.; Cheeseman, J. R.; Scalmani, G.; Barone, V.; Mennucci, B.; Petersson, G. A.; Nakatsuji, H.; Caricato, M.; Li, X.; Hratchian, H. P.; Izmaylov, A. F.; Bloino, J.; Zheng, G.; Sonnenberg, J. L.; Hada, M.; Ehara, M.; Toyota, K.; Fukuda, R.; Hasegawa, J.; Ishida, M.; Nakajima, T.; Honda, Y.; Kitao, O.; Nakai, H.; Vreven, T.; Montgomery, J. A., Jr.; Peralta, J. E.; Ogliaro, F.; Bearpark, M.; Heyd, J. J.; Brothers, E.; Kudin, K. N.; Staroverov, V. N.; Kobayashi, R.; Normand, J.; Raghavachari, K.; Rendell, A.; Burant, J. C.; Iyengar, S. S.; Tomasi, J.; Cossi, M.; Rega, N.; Millam, J. M.; Klene, M.; Knox, J. E.; Cross, J. B.; Bakken, V.; Adamo, C.; Jaramillo, J.; Gomperts, R.; Stratmann, R. E.; Yazyev, O.; Austin, A. J.; Cammi, R.; Pomelli, C.; Ochterski, J. W.; Martin, R. L.; Morokuma, K.; Zakrzewski, V. G.; Voth, G. A.; Salvador, P.; Dannenberg, J. J.; Dapprich, S.; Daniels, A. D.; Farkas, Ö.; Foresman, J. B.; Ortiz, J. V.; Cioslowski, J.; Fox, D. J. *Gaussian 09, Revision C.01*; Gaussian, Inc.: Wallingford, CT, 2010.

(16) (a) Ditchfield, R.; Hehre, W. J.; Pople, J. A. *J. Chem. Phys.* **1971**, *54*, 724–728. (b) Hehre, W. J.; Ditchfield, R.; Pople, J. A. *J. Chem. Phys.* **1972**, *56*, 2257–2261. (c) Hariharan, P. C.; Pople, J. A. *Theor. Chim. Acta* **1973**, *28*, 213–222. (d) Hariharan, P. C.; Pople, J. A. *Mol. Phys.* **1974**, *27*, 209–214. (e) Gordon, M. S. *Chem. Phys. Lett.* **1980**, *76*, 163–168.

(17) Peng, C. Y.; Schlegel, B. *Isr. J. Chem.* **1994**, *33*, 449–454.